HHS Public Access

Author manuscript

Sci Transl Med. Author manuscript; available in PMC 2026 August 13.

Published in final edited form as:

Sci Transl Med. 2026 May 20; 18(850): eadj4902. doi:10.1126/scitranslmed.adj4902.

Real-time in vivo analysis of murine β cells reveals autophagic flux defects before onset of autoimmune diabetes

Olha Melnyk[1], **Charanya Muralidharan**[2], **Bryce E. Duffett**[1], **Alissa N. Muncy**[2], **Leslie E. Wagner**[2], **Matthew Austin**[2], **Jahnavi Aluri**[3], **Abdul S. Qadir**[3], **Yashaswini Battina**[1], **Rachael Morara**[1], **Glorian Perez-Aviles**[2], **Justin J. Crowder**[1], **Michelle M. Martinez-Irizarry**[4], **Sylvaine You**[3,5], **Roberto Mallone**[3,5,6], **Amelia K. Linnemann**[1,2,7,*]

[1] Department of Pediatrics, Indiana University School of Medicine, Indianapolis, IN 46202, USA.

[2] Department of Biochemistry and Molecular Biology, Indiana University School of Medicine, Indianapolis, IN 46202, USA.

[3] Indiana Biosciences Research Institute, Indiana University School of Medicine, Indianapolis, IN 46202, USA.

[4] Department of Medicine, Indiana University School of Medicine, Indianapolis, IN 46202, USA.

[5] Université Paris Cité, Institut Cochin, CNRS, INSERM, Paris, 75005, France.

[6] Assistance Publique Hôpitaux de Paris, Cochin Hospital, Paris, 75005, France.

[7] Indiana Center for Diabetes and Metabolic Diseases, Indiana University School of Medicine, Indianapolis, IN 46202, USA.

Abstract

Autophagy, a vital catabolic process, plays a crucial role in maintaining pancreatic β cell function and is disrupted in established type 1 diabetes. However, it is unclear when and how this critical cell process becomes defective during type 1 diabetes pathogenesis. To study the nature of autophagy dysfunction in the context of autoimmune diabetes, we used real-time intravital microscopy to study autophagic flux in vivo. We generated an AAV8-packaged mCherry-eGFP-LC3B biosensor driven by the insulin promoter for β cell–selective expression. For real-time autophagic flux evaluation, fluorescent signals from eGFP and mCherry fluorophores were correlated in space and time to follow the process of autophagosome-lysosome fusion. We observed autophagic flux defects in the β cells of the nonobese diabetic (NOD) mouse model of type 1 diabetes before hyperglycemia onset at both baseline and in response to interferon-α. These defects were still present, although less apparent, in immunodeficient NOD/*scid/il2rg* (NSG) mice.

*Corresponding author. aklinnem@iu.edu.

Author contributions: A.K.L. obtained funding for these studies and is the guarantor of this work. C.M., O.M., and A.K.L. were responsible for designing the research studies. O.M., C.M., and M.M.M. conducted intravital imaging experiments. B.E.D. and M.M.M. conducted human islet transplantations. O.M., A.N.M, L.E.W., M.A., J.A., A.S.Q., Y.B., R.M., G.P.-A., and J.J.C. conducted in vitro experiments. O.M. conducted data analysis. S.Y. and R.M. contributed materials and helped with data interpretation. O.M., L.E.W., A.N.M., and A.K.L. were responsible for writing the manuscript. All authors contributed to manuscript edits and approved of the submitted version.

Competing interests: A.K.L. has previously served on a scientific advisory board unrelated to this work for the Janssen Research & Development World Without Disease Accelerator T1D Venture. All other authors declare that they have no competing interests.

We also observed heterogeneous autophagic flux in human donor islets transplanted under the kidney capsules of NSG mice. In sum, the ability to visualize autophagic flux in β cells over time in vivo revealed impairments in those β cells that preceded the onset of autoimmune diabetes.

INTRODUCTION

Autophagy is a complex and dynamic process that all cells, including insulin-producing β cells (1, 2), use to degrade and recycle damaged and aging cellular components, including those damaged by reactive oxygen species. During the process of autophagy, cytosolic components are packaged into double-membraned vesicles called autophagosomes and delivered to lysosomes for recycling and degradation (3–5). Functional autophagy is critical for cellular homeostasis and stress response, and defects in autophagy can lead to an accumulation of undegraded cargo and proteins, ultimately leading to apoptosis (6, 7). It is therefore expected that dysfunctional autophagy has been linked to a broad array of human diseases (8), including autoimmune diseases (9). However, excessive autophagy can also lead to cell death (10), highlighting the importance of regulating it within a narrow window to afford its benefits and thereby minimize its negative effects.

Type 1 diabetes (T1D) is an autoimmune disease characterized by immune attack of the insulin-producing pancreatic β cells, leading to their destruction and the development of clinical hyperglycemia. An emerging concept is that β cell dysfunction may play a causative role in T1D pathogenesis by altering the β cell–immune cell crosstalk, thus contributing to the autoimmune attack of β cells (11, 12). We recently observed that autophagy is disrupted in the context of human T1D and that disposal of damaged and dysfunctional β cell components is perturbed in autoantibody-positive human organ donors even before T1D onset (13). These data suggest that defective β cell autophagy may play a causative role in the onset of hyperglycemia, rather than being a mere consequence. We observed histologic evidence of dysfunctional β cell autophagy in a mouse model of spontaneous autoimmune diabetes, the nonobese diabetic (NOD) mouse, before the development of hyperglycemia.

It is well established that disruption of murine β cell autophagy leads to impaired β cell function and glucose intolerance in response to pathological stress (14–16). However, despite indications that defects in autophagy may contribute to β cell dysfunction and autoimmune diabetes pathogenesis, a limitation of prior work is the use of standard approaches to study autophagy, which primarily assess in vivo tissues as snapshots in time (17). Given that autoimmune diabetes development is a stochastic process in both humans and NOD mice, this effectively provides a “moving target” when it comes to determining the relationship between autophagy disruption and β cell dysfunction.

To address this limitation and test whether defective autophagic flux precedes hyperglycemia, we used a β cell–selective fluorescent autophagy biosensor coupled to intravital imaging to visualize β cell autophagic flux in vivo in real time using two-photon microscopy (17–19). We aimed to quantify both baseline and acutely stimulated autophagic flux in the native β cells of NOD mice and immunodeficient NOD/*scid/il2rg* (NSG) mice as well as in human islets transplanted under the kidney capsules of NSG mice. In addition, given the strong association of type I interferons, particularly interferon-α (IFN-α), and

early T1D pathogenesis (20–23), we sought to determine how IFN-α exposure modulates β cell autophagic flux in the models described above. Through this integrated approach, we aimed to define the dynamics of β cell autophagy before clinical onset of diabetes and assess whether alterations in autophagic flux may contribute to early β cell dysfunction in T1D.

RESULTS

An autophagy biosensor successfully labels LC3B protein in the β cell autophagosome membrane in vitro and ex vivo

The set of available fluorescent proteins to study autophagy is constantly growing (24–27), allowing functional assessment of autophagy in addition to more comprehensive observation of different autophagic vesicles. Here, we used a dual-fluorescent biosensor (18, 28) combined with real-time fluorescence microscopy (29) to understand the complex kinetics of autophagic flux in vivo. We used the previously designed (30, 31) dual-fluorescent enhanced green fluorescent protein (eGFP) (32) and mCherry (33) biosensor conjugated to the critical autophagosome membrane component, microtubule-associated protein 1B-light chain 3 (LC3B). eGFP is a green fluorescent protein with enhanced stability in the cytoplasm, but it is sensitive to low pH (34). During autolysosome formation (the fusion of the autophagosome with the lysosome), the eGFP fluorescence is therefore quenched because of the decreased lysosomal pH. Conversely, the red mCherry fluorescence is less sensitive to pH and remains stable during autolysosome formation (Fig. 1A). The biosensor thus changes from emitting both red and green fluorescent signals when the LC3B protein is connected to the autophagosome to carrying the sole red signal when the autophagosome becomes fused with the lysosome.

The eGFP-mCherry-LC3B biosensor was packaged in adeno-associated virus serotype 8 (AAV8) and delivered to β cells, as described using other sensors in our previous work (35). We first validated the biosensor in vitro and ex vivo using rat insulinoma cells [INS-1 832/13 cells (36)], a model cell line for pancreatic β cells (Fig. 1, B and C), the human EndoC-βH1 β cell line (37) (Fig. 1D), isolated mouse islets (Fig. 1E), human islets (Fig. 1F), and human-induced pluripotent stem cell (iPSC)–derived β cells (Fig. 1G). In all systems, detectable biosensor expression was evident within 24 hours of transduction. Consistent with reported autophagosome sizes in primary mammalian cells (0.5 to 1.5 μm) (5), the puncta detected by the biosensor fell within this range, supporting accurate reporting of autophagosome dynamics. In INS-1 cells, we benchmarked flux using complementary manipulations: serum starvation and MSL-7, a small-molecule autophagy stimulator that acts via calcineurin activation and transcription factor E box-binding (TFEB) dephosphorylation (38, 39). Serum starvation typically activates autophagy in many cell types (40, 41); however, it has been reported to block autophagy in INS-1 cells (42, 43). Our biosensor recapitulated this phenotype, with serum starvation decreasing the red/yellow puncta count and increasing the Pearson correlation coefficient (indicative of reduced flux), whereas MSL-7 produced the opposite pattern, an increase in red/yellow puncta and a decrease in Pearson (fig. S1). We then challenged biosensor-expressing cells/islets with additional standard modulators to further assess functionality: bafilomycin A1 [vacuolar H^+-adenosine triphosphatase (v-ATPase) inhibitor] (44, 45), chloroquine (CQ; lysosomal deacidifier) (46, 47), and IFN-α,

a proinflammatory cytokine reported to activate autophagy during early antiviral responses (48, 49). For analysis of autophagic flux, two parameters were quantified. First, the Pearson correlation coefficient of red plus green (red + green) colocalized signal was used to assess the presence of autophagosomes over time in β cells. The ratio of red-only to colocalized (red + green) puncta was used to assess the conversion to autolysosomes and, thus, the rate of autophagosome degradation. During autophagy stimulation, a decrease in the Pearson correlation coefficient (indicating fewer autophagosomes) and an increase in the ratio of red-to-colocalized puncta (indicating more autolysosomes) were expected. Conversely, when autophagy was inhibited, we expected the Pearson coefficient to remain unchanged or to slightly increase and the ratio of red-to-colocalized puncta to remain unchanged.

Across 1 to 3 hours of treatment, inhibitory conditions (bafilomycin and CQ) produced a decrease in the red/yellow ratio with a concomitant increase in Pearson, whereas activation (IFN-α and, similarly, MSL-7) yielded an increase in the red/yellow ratio with a decrease in Pearson (Fig. 1, B to F, and fig. S1). Mirroring the INS-1 results, MSL-7 also stimulated autophagy in EndoC-βH1 cells (fig. S1). Collectively, these data show that coupling a β cell–selective promoter to the eGFP-mCherry-LC3B reporter does not impair sensor performance, that the sensor operates across multiple β cell model systems, and that it enables flux-level readouts, rather than static markers alone, making it useful for interrogating autophagy dynamics.

The autophagy biosensor successfully labels LC3B protein in the β cell autophagosome membrane and can be used to detect flux in vivo

We proceeded to validate the biosensor function in vivo to determine its validity for real-time monitoring of autophagic flux under physiological conditions. A cohort of wild-type C57BL/6J mice was intraperitoneally injected with the AAV8 packaged biosensor, followed by intravital imaging on the native pancreas 3 weeks later. Detectible biosensor expression was observed in several islets throughout the pancreas (Fig. 2A). After this confirmation of sensor expression, mice were retro-orbitally injected with saline and imaged in four dimensions [$X + Y + Z +$ time (XYZT)] to measure the basal level of autophagy, thus providing an internal control for each islet. Autophagic vesicle turnover events have been evaluated previously in immortalized cell lines (50, 51), and these data suggest that autophagic turnover occurs within ~10 to 15 min in these cells. Therefore, taking into consideration the autophagy turnover time frame, images were acquired every 2 min for 30 min to account for one full autophagy turnover process of at least one vesicle in each cell. We can evaluate changes in autophagic flux using compounds that stimulate (IFN-α) or inhibit autophagy (CQ), as demonstrated in vitro above. Therefore, imaging was briefly paused, then these same mice were injected with recombinant mouse IFN-α, and autophagic flux was continually monitored for an additional 20 min (Fig. 2B and movies S1 to S8).

In line with this biosensor readout analysis described above, saline infusion had no effect on autophagic flux, whereas IFN-α infusion rapidly stimulated autophagy. This was evidenced by a reduction in autophagosomes (red + green signal) and a corresponding increase in autolysosomes (red signal normalized to red + green; Fig. 2C, blue profiles). In contrast, in the presence of the autophagy inhibitor CQ, the autophagosomes remained unchanged

after IFN-α treatment, whereas autolysosome levels were reduced and similarly unchanged by IFN-α (Fig. 2C, yellow profiles). To statistically analyze these data, we calculated the ratio of the Pearson coefficient at the final IFN-α time point to the last saline/CQ time points for each animal, because this should allow us to accurately characterize autophagic flux in response to stimulation. Student's *t* test revealed a statistically significant difference between the saline- and CQ-treated groups ($P = 0.0302$), confirming the stimulatory effect of IFN-α on autophagy and the inhibitory properties of CQ (Fig. 2D). The same analysis was applied to the ratio of red-to-colocalized puncta. However, the temporally increased red signal was more variable and therefore not significantly different, likely because of the rapid and cyclical nature of degradation after fusion of the autophagosome with the lysosome.

After imaging, we performed immunofluorescence staining to validate biosensor expression in the collected tissues. Pancreatic tissue collected after imaging with preserved mCherry biosensor expression was stained for insulin and autophagy-related protein 12 (ATG12), an autophagy marker involved in autophagosome formation (52, 53). We observed that all residual mCherry signal in insulin-positive β cells colocalized with ATG12, further confirming that the biosensor specifically targets autophagosomes in the islets and demonstrates β cell selectivity (Fig. 2E).

The autophagy biosensor successfully labels LC3B protein in the β cell autophagosome membrane of NOD mice in vivo

Our prior data from static evaluation of prediabetic NOD mice and autoantibody-positive human donors suggested that autophagic flux may be disrupted before the onset of hyperglycemia (13). Therefore, we turned our attention to determining whether autophagic flux is impaired in NOD mice before hyperglycemia. A series of NOD mice, and immunodeficient NSG mice as a control, was injected with the autophagy biosensor as above. Intravital imaging of the pancreata in NSG mice indicated that islets could be readily identified by biosensor expression (Fig. 3A). Pancreata were collected from a series of animals injected with biosensor and then embedded and sectioned to evaluate infection efficiency throughout the entire pancreas in these models. As demonstrated above (Fig. 2E), the mCherry signal from the biosensor persists upon tissue processing and can be used to mark biosensor-infected cells, whereas insulin antibody can be applied to specifically mark the β cells. We therefore used this approach to quantify infection efficiency and demonstrate localization selectively in the insulin-positive area in the NOD and NSG models (Fig. 3B). Quantification of multiple tissue sections across the entire pancreas revealed a large proportion of β cells expressing biosensor in individual islets (Fig. 3C), which was representative of 40 to 80% of islets throughout the pancreas expressing biosensor in at least 30% of their β cells (Fig. 3D). Collectively, these data demonstrate that the biosensor efficiently infects islets across the mouse strains evaluated through intravital imaging and that the biosensor specifically targets β cells, reinforcing its suitability for studying autophagic flux in β cells.

Autophagic flux is impaired in prediabetic NOD mice in vivo

To investigate autophagic flux in the β cell before diabetes onset, we proceeded to perform intravital imaging of normoglycemic 10-week-old NOD mice injected with the

autophagy biosensor. We included both female and male NOD mice, which develop diabetes stochastically at different rates. Female NSG mice were used as genetically matched controls. During the intravital imaging, pancreatic islets expressing biosensor were identified in the endogenous pancreas as above for the C57BL/6J model, and baseline z-stacks of each selected islet were collected. We then injected a series of mice with saline or CQ followed by IFN-α and collected images over time, as above (Fig. 4A). The Pearson correlation coefficient and punctum count analyses were then performed to assess autophagic flux in four dimensions (XYZT). We observed that IFN-α was able to stimulate a significant reduction in autophagosomes ($P = 0.0254$) and a concomitant, but delayed, increase in autolysosomes in female NSG mice, although these effects were blunted compared with those observed in mice on the B6/J background (Fig. 4B). We observed that female NOD mice exhibited no response to IFN-α, whereas male NOD mice had a reduced, although still significant ($P = 0.0497$), response relative to the NSG controls. Together, these data suggest impaired autophagic flux in the NOD genetic background that is likely further impaired in the presence of autoimmunity. This conclusion is further supported by the inhibition of response to IFN-α by CQ in the β cells of female NSG and male NOD mice but a lack of effect in the β cells of female NOD mice (Fig. 4, C to E). Individual mouse data are presented in fig. S2 (A and B). To better account for the time-dependent nature of these flux changes, we next applied functional data analysis specifically to the Pearson correlation time courses and red/colocalized punctum tracking data for the saline- and IFN-α–treated groups (fig. S2, C and D). Principal components analysis (PCA) was first used to summarize the main temporal pattern, followed by functional analysis of variance (ANOVA) on the full trajectories. This approach, which compares the entire time series rather than a single terminal time point, showed that statistically significant ($P < 0.05$) separation between groups emerged toward the end of the IFN-α injection period. These findings indicate that the late IFN-α time points capture the principal divergence between conditions and therefore support the use of the final Pearson value (IFN-α versus saline/CQ) as a summary measure of autophagic flux. On this basis, the same end-point comparison strategy was applied as a statistical assessment of the IFN-α–evoked response.

To evaluate the level of insulitis in each mouse type, we performed CODEX (codetection by indexing) multiplex imaging (54) using a panel of antibodies specific to pancreatic markers and immune cell markers on pancreata from one animal in each group that underwent intravital imaging (Fig. 5A). Consistent with published studies (55, 56), the level of insulitis was most prevalent in female NOD mice. As expected, NSG mice did not show any signs of insulitis. However, insulin-positive cells were still present in all mice, confirming the continued presence of β cells despite immune infiltration and further demonstrating that the defective autophagic flux observed in vivo represents these residual β cells in the infiltrated islets. We quantified the numbers of $CD8^+$ and $CD3^+$ cells around all visible islets and included major histocompatibility complex (MHC) class I staining as an additional cell stress indicator in each mouse strain using the high-resolution, multiplexed capabilities of the CODEX system. These data confirmed a more advanced prediabetic state in the female NOD mice compared with NSG mice, whereas males showed no significant enrichment (Fig. 5, B and C; $CD3^+$ $P = 0.0032$; $CD8^+$ $P = 0.0109$). We also performed standard immunohistochemistry on pancreata from the mice subjected to intravital imaging,

computed a per-mouse insulitis score (see Materials and Methods), and correlated it with each animal's intravital autophagy response, quantified as the saline–to–IFN-α change in Pearson colocalization (Pearson fold change; Fig. 5D) and in the red/yellow punctum metric (punctum fold change; Fig. 5E). Per-animal scatterplots with Spearman correlations indicated that greater insulitis burden was not consistently associated with a weaker IFN-α response. These data support the conclusion that immune infiltration contributes only modestly to impaired autophagic flux in individual NOD mice. Collectively, these results demonstrate impaired β cell autophagic flux before the onset of hyperglycemia in NOD mice that is not predictable by the degree of active insulitis alone.

Autophagic flux is heterogeneous in human islet β cells in an in vivo setting

Many limitations preclude the in vivo study of islet autophagic flux in the human pancreas. However, as a proxy to studying human β cells in their native niche, our approach to studying autophagic flux in vivo in real time can also be used to study human β cells by transplanting them into NSG mice. Although human islets can be effectively transplanted in several sites (57), one of the most successful and easily accessible sites is the space under the kidney capsule. We therefore transduced human donor pancreatic islets ex vivo with the autophagy biosensor and then transplanted them under the kidney capsules of NSG mice. Islets from each individual donor were transplanted into four mice. After 2 weeks to allow for islet engraftment, mice were subjected to intravital kidney imaging of the transplanted islets (Fig. 6A).

Using a similar treatment approach as above for the mouse pancreas, we proceeded to evaluate autophagic flux in the transplanted human islets. For each donor (Table 1), a set of animals was first injected with saline to evaluate baseline autophagic flux, followed by an injection of recombinant human IFN-α to stimulate autophagy and allow for four-dimensional (4D; XYZT) imaging. A parallel set of islet-engrafted mice was injected with CQ before IFN-α. When evaluating all donors together (Fig. 6B), we observed a modest stimulation of autophagic flux by IFN-α ($P = 0.0192$) compared with what was observed with native mouse islets, which was abolished by CQ (Fig. 6C).

It is well established that interindividual variability between human donors can affect islet physiology and function (58). Therefore, we also evaluated autophagic flux in each donor individually. When individual donor data were plotted (Fig. 6, D and E), we observed a heterogeneous response to IFN-α, which was consistently abolished by CQ for all donors. Ex vivo analysis of human islet autophagy stimulation by IFN-α confirmed the ability of IFN-α to acutely stimulate flux, as evidenced by a significant increase in LC3:LAMP1 (lysosome associated membrane protein 1) colocalization within 15 min (Fig. 6F; $P = 0.0001$) using an antibody-based approach, we previously validated for quantification of flux (13). Consistent with these findings, quantification of LC3 puncta and LAMP1 puncta in the insulin-positive area demonstrated increased autophagosome formation and lysosomal engagement after IFN-α treatment (Fig. 6F; LAMP1 $P = 0.0025$, LC3 $P = 0.0001$), with representative images shown in Fig. 6G. In contrast, p62 levels in the insulin-positive area remained largely unchanged at this early time point (Fig. 6H), despite induction of autophagic flux. This likely reflects the short duration of IFN-α exposure and the temporal

delay between autophagosome formation and measurable cargo degradation, suggesting that p62 turnover may not yet be detectable under these acute conditions. However, use of the biosensor revealed a more heterogeneous real-time response between donors, likely reflective of the dynamic system and suggesting that the in vivo heterogeneity is unlikely to be due to engraftment efficiency (fig. S3). Collectively, these data demonstrate that autophagic flux can be stimulated by IFN-α in human islets similar to that in mouse pancreatic islets and that this can be imaged in an in vivo setting in real time.

DISCUSSION

T1D has classically been viewed solely as an immune-driven disease. However, emerging evidence suggests that β cells may play an active role in their own demise (59–61). Autophagy plays an important role in β cell homeostasis and survival (1). Autophagy has been extensively studied in the context of type 2 diabetes, β cell homeostasis (2), and endoplasmic reticulum stress response (62). However, autophagy has only recently been investigated in the context of T1D (63), and we ultimately know very little about the role of β cell autophagy in human disease pathogenesis.

Multiple approaches can be used to study autophagy such as collection and preservation of tissues for further investigation with established techniques of immunofluorescence, Western blotting, and electron microscopy (17, 18, 64). However, limitations exist in that many of these approaches provide only a static snapshot of the dynamic autophagy process. Virally packaged fluorescent biosensors are a useful and versatile alternative to study dynamic processes, and we have previously used this approach successfully to evaluate reactive oxygen species dynamics and calcium oscillations in β cells in vivo (35, 57, 65, 66). Fluorescent autophagy sensors have also been used successfully to study autophagic flux in β cells in vitro by us and others (67, 68). Therefore, we reasoned that this approach could be used to enable the investigation of the dynamic nature of autophagy and allow the visualization of autophagic flux in vivo.

Autophagy sensors have been used to evaluate autophagy in vivo using isolated tissues from transgenic mice (69, 70). Although these studies provide useful information, they fall short in truly evaluating real-time dynamic autophagic flux in the presence of systemic modulators. Here, we have coupled the use of a validated β cell–selective dual-fluorescent biosensor with intravital imaging to interrogate the dynamics of autophagic flux in real time in vivo. The use of viral packaging of the sensor allows us to study β cell autophagy in any mouse model or in isolated islets with high infection efficiency but without complicated breeding to genetically introduce the sensor or the risk of negative consequences from prolonged expression of multiple fluorescent proteins (Fig. 3). We therefore used this versatile approach to selectively study β cell autophagic flux in vivo in both native mouse islets and xenografted human islets.

To study autophagy dynamically in the context of T1D, we used the NOD mouse model of spontaneous autoimmune diabetes. Using both male and female mice, we evaluated β cell autophagy at different stages of the immune attack on pancreatic islets before diabetes onset in the NOD mice. We chose to inject animals with the cytokine IFN-α because of

its established relevance to human T1D pathogenesis (22, 23), with the hypothesis that it should stimulate autophagic flux as part of the innate response preceding hyperglycemia but only under conditions where autophagy is able to be physiologically stimulated. Our testing in wild-type C57B6/J mice demonstrated the stimulation of β cell autophagy by IFN-α. However, we observed an impairment in autophagic flux by IFN-α in prediabetic female NOD mice compared with age- and sex-matched NSG controls. This demonstrates that autophagy is impaired before diabetes onset in the NOD model, consistent with our previous ex vivo observations using pancreas tissue sections from NOD mice and islets of autoantibody-positive human donors (13).

Although these previous observations established that autophagy is defective before diabetes onset in the NOD model, whether autoimmunity affects autophagy suppression remained unaddressed. In other words, our previous work was unable to fully distinguish between the effects of genetic predisposition and immune-mediated repression of β cell autophagy. Therefore, we evaluated autophagic flux in age-matched male NOD mice. It is well known that male NOD mice develop diabetes much later and with a lower penetrance than females (55), concomitant with reduced insulitis. We observed increased stimulation of autophagic flux by IFN-α in the β cells of male versus female NOD mice. However, the ability to stimulate autophagy in these animals was still somewhat repressed compared with that in NSG and C57B6/J mice. These observations may suggest a combination of genetics and autoimmunity that contributes to autophagy suppression in the NOD model.

Although human islets cannot be studied in vivo in the same way as mouse islets for ethical reasons, human islets are widely studied in an in vivo context after transplantation into NSG mice (57). Therefore, we used this approach to perform real-time 4D autophagy monitoring in human β cells in intact islets in an in vivo setting after transplantation under the kidney capsules of NSG mice. Using IFN-α, we observed that although we could sometimes stimulate autophagic flux, there was substantial donor heterogeneity in autophagy in the nondiabetic donors evaluated. This is perhaps expected and may be reflective of interindividual biological variability that is not replicated in inbred mouse models. Nonetheless, we demonstrated an ability to stimulate autophagic flux in human islets in vivo, thus establishing our platform for future studies in islets from donors with clinical or preclinical (autoantibody-positive) T1D and for testing therapeutic autophagy modulators.

Several limitations of this study should be considered. First, although our findings demonstrate impaired β cell autophagic flux before hyperglycemia, direct causality between autophagy defects and diabetes progression cannot be established using the current models. Additional longitudinal studies will be required to determine whether impaired autophagic flux is a driver or a consequence of disease development. Second, although transplantation of human islets into NSG mice enables in vivo analysis, islet isolation and engraftment may introduce cellular stress that could influence autophagic responses. Metabolic stress has been reported to modulate autophagic activity in a heterogeneous manner (70, 71), which may contribute to the variability observed across human donors. Last, although donor-dependent differences in IFN-α–induced autophagic flux were observed, the factors underlying this heterogeneity remain to be defined. Future studies incorporating longitudinal

imaging approaches and well-characterized donor cohorts will be important to address these questions and further clarify the role of autophagy in T1D pathogenesis.

In summary, we demonstrate in four dimensions that β cell autophagic flux is impaired before hyperglycemia in an established model of autoimmune diabetes. Furthermore, we can monitor human β cell autophagy in four dimensions in an in vivo setting. Collectively, our observations raise important questions regarding how impaired autophagic responses to IFN-α may contribute to early β cell dysfunction and the progression of autoimmunity and provide a platform for evaluating the efficacy of therapeutic strategies aimed at restoring this critical process. The potential for studies such as these to evaluate not only acute drug response but also long-term response and functional outcomes through the incorporation of abdominal imaging windows (35, 72, 73) remains to be addressed. However, we anticipate that future studies grounded in this work will contribute to our understanding of T1D pathogenesis.

MATERIALS AND METHODS

Study design

This study was designed to dynamically assess autophagic flux in vivo in endogenous mouse pancreatic β cells and in transplanted human β cells. The overall goal was to determine whether defective β cell autophagic flux precedes the onset of hyperglycemia and to evaluate how IFN-α modulates autophagic flux in models relevant to T1D. We hypothesized that dynamic in vivo assessment of β cell autophagic flux would reveal early defects associated with autoimmune diabetes pathogenesis and define β cell responses to IFN-α. Sex was considered as a biological variable during the planning of all animal experiments. Male and female NOD mice and female NSG mice were used as indicated for each experiment. Human islets from both male and female donors were included in transplantation studies, as indicated in Table 1. All animal experiments were approved by the Indiana University School of Medicine Institutional Animal Care and Use Committee. Mice were housed in a temperature-controlled facility with a 12-hour light/12-hour dark cycle and were given free access to food and water. C57BL/6J (RRID:IMSR_JAX:000664) and NOD (RRID:IMSR_JAX:001976) mice were purchased from the Jackson Laboratory at 6 weeks of age. NOD.Cg-Prkdc^{scid} Il2rg^{tm1Wjl}/SzJ (NSG; RRID:IMSR_JAX:005557) mice were obtained from the on-site breeding colony at the Preclinical Modeling and Therapeutics Core at the Indiana University Simon Comprehensive Cancer Center at 6 weeks of age. Blood glucose in NOD mice was monitored biweekly with an AlphaTrak2 glucometer (Zoetis), and animals were classified as diabetic after 2 consecutive days of blood glucose readings greater than 250 mg/dl. For biosensor imaging studies, male and female NOD mice and female NSG mice were injected at 7 weeks of age with ~2.31×10^{12} genome copies (GC) of AAV8 biosensor, and intravital imaging was performed at 10 weeks of age. All animals from which imaging data were collected were included in the final analysis. Human islets used in this study were deidentified specimens exempt from Institutional Review Board approval and were obtained through the Integrated Islet Distribution Program (IIDP) or the Alberta Diabetes Institute IsletCore. All experiments were performed with at least three biological replicates. For human islet studies, a biological replicate was defined as islets from an

individual donor, whereas for cell line–based studies, a biological replicate corresponded to an independent passage of cells. Several experiments also included technical triplicates to assess consistency in individual donor islets. Statistical significance was determined on the basis of biological replication. Image analysis was performed in a blinded manner to minimize bias.

Generation of a β cell–selective fluorescent autophagy biosensor

AAV8 has previously been shown to have pancreas tropism (74), and we previously used a hybrid insulin/rabbit β-globin promoter (75), which we refer to as RIP1, to enable β cell–selective sensor expression in vivo (35). Here, we generated AAV8-RIP1-mCherry-EGFP-LC3B plasmid by cloning the insulin/β-globin promoter and the mCherry-EGFP-LC3B construct [from Addgene construct no. 22418; (31)] into an AAV8 packaging plasmid. The plasmid was then packaged into the AAV8 at the Vector Core of the Gene Therapy Program at the University of Pennsylvania.

Transduction of cell lines, islets, and iPSC-derived β cells

INS1 cells were cultured and maintained in RPMI 1640 medium supplemented with 10% fetal bovine serum (Gibco, catalog no. A5256701), 10 mM Hepes (Gibco, catalog no. 15630080), 2 mM L-glutamine (Gibco, catalog no. 25030081), 1 mM sodium pyruvate (Gibco, catalog no. 11360070), 0.05 mM 2-mercaptoethanol (Gibco, catalog no. 21985023), and 1% antibiotic-antimycotic (Gibco, catalog no. 15240062). Cells were transduced with AAV8-RIP1-mCherry-EGFP-LC3B at a multiplicity of infection (MOI) of 5000 for 24 hours. After transduction, the viral medium was removed, and cells were treated with autophagy modulators on the microscope stage during imaging for 1 hour. Throughout imaging, cells were maintained at 37°C with 5% CO_2. Autophagy was modulated by treating cells with mouse recombinant IFN-α (2000 IU/ml; BioLegend, catalog no. 752802) or 100 nM bafilomycin A1 (Sigma-Aldrich, catalog no. B1793) or 50 nM of wortmannin (MedChemExpress, catalog no. HY-10197).

EndoC-βH1 cells were cultured as previously described (37). Briefly, cells were maintained on plates coated with Matrigel (100 mg/ml; Corning, catalog no. 356237) and fibronectin (2 mg/ml; Sigma-Aldrich, catalog no. F1141) in Dulbecco's modified Eagle's medium (5.6 mM glucose) supplemented with 2% albumin from bovine serum fraction V (Equitech-Bio, catalog no. BAH66) [bovine serum albumin (BSA)], nicotinamide (10 mM; Sigma-Aldrich, catalog no. N0636), transferrin (5.5 mg/ml; Sigma-Aldrich, catalog no. T8158), sodium selenite (6.7 ng/ml; Sigma-Aldrich, catalog no. S5261), 2-mercaptoethanol (50 mM; Sigma-Aldrich, catalog no. M3148), and penicillin/streptomycin (100 U/ml and 100 mg/ml, respectively; Thermo Fisher Scientific, catalog no. 15140122). Passages were performed weekly, and mycoplasma contamination was periodically tested (Applied Biological Materials). During 1 hour of imaging, cells were kept at 37°C with 5% CO_2 and treated with human recombinant IFN-α (2000 IU/ml; Novus Biologicals, catalog no. NBP2–26551), 100 nM bafilomycin A1 (Sigma-Aldrich, catalog no. B1793), or 100 μM MSL-7 (Axon Medchem, 2932).

Mouse islets were isolated after enzymatic digestion of the pancreas with collagenase, prepared by the IU Diabetes Center Islet Core as previously described (76) or isolated in house using a Ficoll gradient. Briefly, the pancreas was inflated with collagenase solution [0.75 to 1 mg/ml; in Hanks' balanced salt solution (HBSS)/0.02% BSA], dissociated in a 37°C shaking water bath. Islets were washed in ice-cold HBSS/0.02% BSA and filtered through a 500-μm mesh to remove debris. Islets were further purified with a Ficoll gradient, then washed with HBSS/0.02% BSA, and resuspended in islet medium containing RPMI (no glucose; Gibco, catalog no. 11875093) with 6.7 mM glucose, 8% heat-inactivated fetal bovine serum (Gibco, catalog no. 16140071), and 0.8% penicillin-streptomycin (Gibco, catalog no. 15140122). Islets were cultured at 37°C with 5% CO_2 and rested overnight before experimentation.

Human islets were obtained from the IIDP or the Alberta Diabetes Institute Islet Core. They were cultured in Prodo islet medium (5.8 mM glucose; Prodo, catalog no. PIM-S001GMP) with 5% human AB serum supplement (Prodo, catalog no. PIM-ABS001GMP), 1% glutamine and glutathione supplement (Prodo, catalog no. PIM-G001GMP), and ciprofloxacin (10 μg/ml; Thermo Fisher Scientific, catalog no. MT61277RG). Upon receipt, the islets were centrifuged at 350*g* for 5 min, resuspended in complete islet medium, and allowed to recover overnight before infection with the AAV8-packaged biosensor.

After overnight recovery, mouse and human islets were suspended in Accutase (Innovative Cell Technologies, catalog no. AT-104) and incubated for 1 min at 37°C to loosen, but not fully dissociate, the cells, thus enhancing biosensor infection efficiency. The enzyme was inactivated with serum-containing medium. Islets were then transduced with AAV8-RIP1-mCherry-EGFP-LC3B at an MOI of 5000 for ~16 to 18 hours at 37°C in fresh complete islet medium. During 1 hour of imaging, islets were maintained at 37°C with 5% CO_2 and treated with recombinant human IFN-α (2000 IU/ml; Novus Biologicals catalog no. NBP2–26551) or recombinant mouse IFN-α (BioLegend, catalog no. 752802), along with 20 μM CQ diphosphate (Thermo Fisher Scientific, catalog no. J64459.14).

Undifferentiated human pluripotent stem cells (iPSCs) were maintained in Essential 8 (E8) medium (Thermo Fisher Scientific, catalog no. A1517001) on Matrigel-coated plates and passaged using EDTA. β cell differentiation was carried out using a six-stage protocol, which includes the definitive endoderm, primitive gut tube, pancreatic progenitor stage (S)1, pancreatic progenitor S2, pancreatic endocrine, and lastly mature stem cell (SC) islet cells (77). For differentiation, iPSCs were dissociated with EDTA and seeded onto new Matrigel-coated plates in E8 medium supplemented with 10 μM Y-27632 (Rho-associated kinase inhibitor; Tocris Bioscience, catalog no. 1254) at a density of 2.0 to 2.5 × 10^6 cells per well in six-well plates. To initiate stage 1 (definitive endoderm) differentiation, the medium was replaced with D0 medium, consisting of basal medium 1 with activin A (100 ng/ml; MedChemExpress, catalog no. HY-P703994) and CHIR99021 (500 nM; Sigma-Aldrich, catalog no. SML1046). On day 1, cells were fed again with D0 medium, followed by refeeding on days 2 and 3 with basal medium 1 containing only activin A. The further differentiation from S2 to S6 followed the stepwise protocol detailed by Hogrebe *et al.* (77). Medium changes were performed daily until S5, with medium refreshed every other

day beginning on the first day of S6. Treatments were performed exactly as above during 1 hour of live imaging.

Transduction of native mouse islets

To induce β cell–selective expression of the RIP1-mCherry-EGFP-LC3B biosensor, animals were given intraperitoneal injections of AAV8-packaged sensor 3 weeks before the intravital imaging session. All injections were given to animals at 7 weeks of age and between 9:00 a.m. and 11:00 a.m. to ensure consistency of sensor expression in the tissue. This enabled robust expression of sensor specifically in the pancreatic β cells that lasted for at least 20 weeks beyond the injection time (fig. S4).

Transplantation of human islets

After transduction as described above, human islets were centrifuged at 350*g* for 5 min, and viral islet medium was removed. The islets were then transferred to virus-free islet medium and transplanted under the left kidney capsules of NSG mice. Approximately 1000 IEQ (islet equivalents) were transplanted per mouse. Briefly, mice receiving the transplants were subcutaneously treated with Ethiqa XR (3.25 mg/kg; 800-MIDWEST product number 267.10000.3) before starting the surgery. During the surgery, mice were anesthetized through isoflurane inhalation and kept on a warming blanket until they regained reflexes postsurgery. The left flank of the mouse (around the kidney area) was shaved, and excess hair was removed with Nair hair removal cream (Church & Dwight Co. Inc.). The shaved area was cleaned with an alcohol swab, a small incision on the skin was created, and the left kidney was gently externalized. The distal end of a sterile polyethylene (PE-50) tubing was attached to a Hamilton screw syringe containing a blunt needle tip. The tubing containing the islets was cut at an angle to make the tubing beveled. Then, a small nick was made on the kidney capsule with a 30-gauge needle, and the beveled end of the tubing containing the islets was carefully placed under the kidney capsule, all while keeping the tissue moist with saline. Then, a small air bubble was delivered very carefully and slowly under the capsule followed by islets. The kidney was then placed back into the peritoneal cavity, and the muscle and skin were sutured using 5–0 VICRYL sutures. After surgery, the animals were treated with analgesics/anti-inflammatories and were monitored until they regained reflexes. The animals were singly housed in a clean cage and provided with wet feed and were subcutaneously administered carprofen (5 μg/kg) as necessary for pain management postsurgery.

Intravital imaging of endogenous mouse pancreas

Mice were anesthetized by isoflurane inhalation, then a small flank incision was made, and pancreata were gently externalized as we have previously described (35). Each animal was placed such that the externalized pancreas could rest on the surface of a glass-bottom imaging dish (0.17-mm thick, 40 mm in diameter; WillCo, catalog no. GWST-5040). The temperature and humidity of the externalized organ were monitored throughout the imaging session. Throughout the surgery and imaging, ophthalmic ointment was applied to avoid drying of the animal’s eyes. To reach the deeper pancreas tissue, two-photon microscopy was used, with penetration depth reaching from 500 μm up to 1 mm into the tissue (78, 79). Animals were imaged using a Leica TCS SP8 DIVE confocal multiphoton system mounted on an inverted stand equipped with a Spectra-Physics MaiTai DeepSee laser and mounted

with a 40× 1.1 numerical aperture (NA) water objective. Intraperitoneal and retro-orbital injections were performed on the animals during the imaging. Initially, pancreatic islets were identified through the eyepiece by looking for the “red” and “green” fluorescence of the β cells expressing the autophagy biosensor. We collected 512 pixel–by–512 pixel images at 400-Hz scanning frequency with 900- and 1050-nm wavelength excitation lasers, whereas emission signal from the biosensor was collected on the Power HyD detectors at 490- to 530-nm and 575- to 625-nm emission windows for eGFP and mCherry signals, respectively. Next, a baseline 4D z-stack of each selected islet was collected (2- to 3-μm thick) nonstop for a duration of 3 min. After this, animals were intraperitoneally injected with 100 μl of saline or CQ diphosphate (50 mg/kg; Tocris Bioscience, catalog no. 4109), and a selected islet was imaged for a total duration of 30 min, with images collected at time intervals of 2 min. Animals were then given retro-orbital injections of 2.75×10^5 IU of recombinant mouse IFN-α (BioLegend, catalog no. 752802), and the final 20 min of images with the same time intervals was collected. To evaluate islet architecture, retro-orbital injection of albumin conjugated with Alexa Fluor 647 was performed at the end of saline/CQ/IFN-α imaging. Images of the vasculature were collected using an 840-nm laser wavelength, with emission collected in the 650- to 700-nm wavelength window of the photomultiplier tube detector.

Analysis of intravital images

Images were collected in sequential order: The first excitation of the 900-nm laser was set, and appropriate emission spectra were collected; the next 1050-nm laser excitation was set. The images were collected sequentially between laser lines, but fast switching allowed overall image collection to be performed almost simultaneously. FIJI was used for all analyses (80). The maximum intensity projection of the collected z-stacks of the islet was created first for further image analysis. Collected image channels from 900-nm laser excitation and 490- to 530-nm emission and 1050-nm laser excitation and 575- to 625-nm emission were then separated and analyzed for colocalization and punctum count. As an initial step, background subtraction was performed on both images: Image background was identified in the places of images where no signal was visible, and the average intensity of background pixels was subtracted from the whole image. Next, rolling ball background subtraction was performed with the FIJI plugin, of radius 25 pixels. For the red and green colocalization in space, the Pearson correlation coefficient was measured for the selected images using the colocalization threshold plugin in ImageJ. The Pearson correlation coefficient for the positive area was used as a measured parameter. Next, a median filter was applied to the images for punctum identification in both channels. Using the Image calculator plugin in FIJI, the “and” image of red and green channels was created (only pixels that have positive intensity simultaneously in both channels are shown) and identified as a colocalized signal. The particles analysis plugin in ImageJ was then used to calculate puncta. To avoid punctum overcounting, a percentage of the positive area was used as a measuring parameter for the punctum count. The red-only image was created as a difference between colocalized and red signal images, to count only red puncta that did not have green signal associated with them. The same particle analysis plugin was used to count the red-only puncta. Next, the ratio of the red-only/colocalized puncta was plotted for each time data

point. Last, data were represented as a fold change of the time 0 data point (baseline image collected for 3 min before any injections were administered to the animals).

The Pearson correlation coefficient is insensitive to the intensity difference between two channels; thus, we only analyzed the co-occurrence in space of the two fluorophores. The punctum count specifically evaluates the autophagic flux. With an increase in the autophagic flux, the number of red puncta will increase and that of yellow will decrease simultaneously, leading to an increased ratio. In the case of autophagy inhibition with CQ, the number of red puncta will not change significantly, but the number of yellow puncta will increase, leading to a decreased ratio.

For each image and each outcome (Pearson correlation; red-only/colocalized punctum ratio), we treated the 60-min acquisition as a single continuous time course (saline or CQ first and then IFN-α). Per-cell trajectories were converted to smooth functions. We first compared mouse models with principal components of the functional data [PCA of smoothed curves; functional principal components analysis (FPCA)] to visualize dominant temporal patterns (PC2 panels shown). To identify when models differed, we performed a functional ANOVA using a permutation, max-T procedure: At each minute, we computed the classical F-statistic across mouse models and obtained family-wise error–controlled P values from the permutation distribution of the maximum F over time. Figures display $F(t)$ with top peaks highlighted and a reference for $P < 0.05$.

For summary treatment effects, we compared end points in the same groups: the last time point before IFN-α (end of saline/CQ) versus the last recorded time point after IFN-α. Changes were tested by paired t test. Statistical analyses were conducted in R (version ≥4.2) using the fda, tidyverse, and mgcv packages, with a custom script to generate the functional ANOVA curves and FPCA panels.

Immunofluorescence staining of mouse islets after intravital imaging

After imaging, pancreata were collected and flash-frozen in optimal cutting temperature (OCT) compound (Thermo Fisher Scientific, catalog no. 23–730-571). OCT compound–embedded pancreata were sectioned at 8-μm thickness, and then the tissues were permeabilized with 1% phosphate-buffered saline (PBS) containing Triton X-100 (Thermo Fisher Scientific, catalog no. AAA16046AP) for 15 min. Slides were then blocked with Dako blocking buffer (Agilent Technologies, catalog no. X0909) before incubation with antibodies in Dako antibody diluent (Agilent Technologies, catalog no. S3022) overnight at 4°C in a humidified chamber with the following primary antibodies: guinea pig anti-insulin antibody (1:250; Bio-Rad, 5330–0104G) and rabbit ATG12 antibody (1:100; Cell Signaling Technology, D88H11). After overnight incubation, the slides were washed with PBS, and secondary antibodies goat anti-guinea pig Alexa Fluor 647 (Invitrogen, catalog no. A-21450) or donkey anti-rabbit Alexa Fluor 488 (Invitrogen, catalog no. A-21206) were added at 1:500 dilution together with 4′,6-diamidino-2-phenylindole (DAPI; Thermo Fisher Scientific, catalog no. D1306) at a 1:2000 dilution to stain nuclei. The slides were incubated in the dark with secondary antibodies for 1 hour at room temperature and then mounted using a hard-set mounting medium (Everbrite, catalog no. NC0965689). All images were acquired using a Zeiss LSM 700 confocal microscope, with 40× 1.3 NA oil objective.

Collected 10-μm-thick z-stacks (with 1-μm step) of the islet images from the tissue slices were projected as a maximum intensity on one plane, then background subtraction was performed (by measuring the mean intensity of the not fluorescent part of the image and subtracting that value from the whole image) for all channels separately, and an insulin mask was created to measure the insulin area. The insulin mask was then applied over the mCherry channels, and the area of each signal was calculated over the insulin mask. Data are presented as a ratio of each channel area over the insulin-positive area.

CODEX staining of the mouse tissues after intravital imaging

After intravital imaging, mouse tissues (pancreas and spleen) were flash-frozen in OCT on a bed of dry ice. Tissues were sectioned at a thickness of 8 μm and mounted onto positively charged microscope slides precoated with CellTak (Corning, catalog no. 354240) at a concentration of 3.5 $\mu g/cm^2$ of the slide surface area. CODEX staining was then performed according to the manufacturer's instructions for the PhenoCycler/PhenoImager platform (Akoya Biosciences) (81), using a multiplex antibody panel against pancreatic and immune cell markers. After completion of the automated staining and fixation steps, flow cells were mounted, and slides were equilibrated in 1× PhenoCycler buffer (Akoya AKO-AR600250ML) before imaging on the PhenoCycler Fusion system. The following antibodies are shown: rabbit anti-insulin antibody (EPR17359)—BSA and azide free (Abcam, catalog no. ab202760), rabbit anti-glucagon antibody (EP3070)—BSA and azide free (Abcam, catalog no. ab167078), mouse anti-MHC class I (BioLegend, catalog no. 114602), anti-CD3 (Akoya, catalog no. 4550109), and anti-CD8 (Akoya, catalog no. 4250017).

Immunohistochemistry and insulitis scoring

Frozen pancreas tissue sections from mice exposed to intravital imaging were equilibrated to room temperature and then fixed/permeabilized in ice-cold methanol for 20 min. Endogenous peroxidase activity was quenched using freshly prepared methanol containing 0.45% H_2O_2, sections were blocked with Dako blocking buffer (Agilent Technologies, catalog no. X0909) in a humidified chamber, and then slides were incubated overnight at 4°C with primary antibody [1:200; rabbit anti-CD3 epsilon antibody (SP7), Abcam). The next day, slides were incubated with SignalStain Boost IHC Detection Reagent (rabbit; Cell Signaling Technology, catalog no. 18653). Color development was performed with DAB Substrate Working Solution (Cell Signaling Technology DAB Kit, catalog no. 8059) for up to 10 min until the desired signal intensity was reached. Sections were counterstained with a Hematoxylin and Eosin Staining Kit according to the manufacturer's instructions (Vector Laboratories, catalog no. H-3502). Slides were then mounted with Permount mounting medium (Thermo Fisher Scientific, catalog no. SP15–100) before imaging on a Keyence BZ-X810 microscope in brightfield using a 10× 0.3 NA objective.

For each section, tissue boundaries were registered via the instrument's MultiPoint stitching workflow; autofocus, autobrightness (with manual refinement), and white balance were applied before capture. Images were acquired with z-stack autofocus capture, stitched, and then exported at original scale. The micrometer-per-pixel calibration was recorded from the BZ-Analyzer "Scale" settings and used downstream for analysis. Whole-slide images were

analyzed in QuPath. Images were set to Brightfield H-DAB, and stain vectors (hematoxylin, DAB, and background) were standardized by sampling representative regions of interest for each slide. Islets were annotated manually, and a 50-μm peri-islet region was generated by expanding each islet annotation. Positive cell detection was run with the requested pixel size matched to the Keyence calibration; nuclei per cell expansion was set to ~1 to 2 μm. Insulitis scoring was derived per islet and aggregated per mouse after established criteria (82, 83).

Intravital imaging of human islets

A similar procedure as the intravital imaging for mouse pancreata was performed for the human islet imaging. During the surgery before the imaging session, mice under inhaled isoflurane anesthesia underwent gentle externalization of the left kidney, which was placed on the glass-bottomed imaging dish. The kidney was kept moist throughout all procedures with saline, and the temperature of the imaging dish was kept near body temperature levels (36° to 37°C). Next, each animal was placed on the microscope and imaged using a 25× 0.95 NA water objective. Transplanted human islets were identified first through the eyepiece, and then a z-stack of 2- to 3-μm-thick slices was imaged for 3 min nonstop at a 400-Hz frequency to obtain a baseline sensor readout. Intraperitoneal injection of the saline or CQ was performed as above, and then a chosen islet was imaged for 30 min at 2-min time intervals. Next, retro-orbital injection of recombinant human IFN-α (2.75×10^5 IU; Novus Biologicals, catalog no. NBP2–26551) was performed, and the last 20 min of images of the same islet at the same time interval was collected.

In vitro analysis of autophagy in human islets

Human islets (1000 IEQ per treatment group) were treated with either PBS or IFN-α (2000 IU/ml; Novus Biologicals, catalog no. NBP2–26551) for 15 min. After treatment, islets were washed three times with PBS and fixed with 4% paraformaldehyde. Fixed islets were then cryoprotected in 30% sucrose at 4°C overnight, embedded in OCT, and sectioned at 6-μm sections. The sections were then subjected to immunofluorescence staining after blocking and permeabilization and incubated with primary antibodies overnight at 4°C against LAMP1 (1:100; BD Biosciences, catalog no. 555798), LC3 A/B (1:100; Cell Signaling Technology, catalog no. 12741), SQSTM1 (p62) (1:100; Abcam, catalog no. ab91526), and insulin (1:2; Dako, catalog no. IR002). Secondary antibodies were diluted 1:500 in antibody diluent (Abcam, catalog no. 64211) and incubated at room temperature for 1 hour: Alexa Fluor 647 donkey anti-rabbit immunoglobulin G (IgG), Alexa Fluor 594 goat anti-mouse IgG, and Alexa Fluor 488 goat anti-guinea pig IgG. DAPI was used to stain the nuclei. Images were acquired using a Leica Stellaris confocal microscope with 40× 1.3 NA oil objective. Collected z-stack images of human islets (~10-μm total thickness, 1-μm step size) were projected into a single plane using maximum intensity projection. Background subtraction was performed independently for each channel by measuring the mean intensity of a nonfluorescent region and subtracting this value from the entire image. An insulin mask was generated by thresholding the insulin channel, and this binary mask was used to restrict all subsequent analyses. The insulin mask was applied to the LC3, LAMP1, and p62 channels to quantify signal specifically in β cells. For LC3 and LAMP1 analysis, puncta were identified after median filtering to reduce noise. LC3 puncta and LAMP1 puncta were quantified in the insulin-positive area using the analyze particles function in FIJI, with

consistent thresholding parameters applied across all conditions. Colocalization between LC3 and LAMP1 was assessed using the image calculator to generate an “and” mask, and the resulting signal was quantified as a measure of autophagosome-lysosome interaction. For p62 analysis, total fluorescence in the insulin-positive area was measured after background subtraction. All measurements were normalized to the number of nuclei presented in the image.

Statistical analysis

Individual-level data are provided in data file S1. Statistical analyses were performed using GraphPad Prism (version 11.0.0, GraphPad Software) and R (version ≥4.2). For comparisons between two groups, Student’s *t* test was used, and for multiple-group comparisons, one-way ANOVA followed by Dunnett’s or Tukey’s post hoc test was applied, as appropriate. Normality of data distributions was assessed using the Shapiro-Wilk test and by visual inspection of Q-Q and frequency distribution plots. When repeated measures were present, mixed-effects ANOVA was used. For intravital imaging data, time-resolved measurements of the Pearson correlation coefficient and red-only/colocalized punctum ratio were analyzed as continuous trajectories. Functional data analysis was performed by first smoothing individual time courses, followed by FPCA to identify dominant temporal patterns. Group differences across time were assessed using functional ANOVA with a permutation-based max-T procedure to control for family-wise error across time points. To summarize treatment effects, end-point comparisons were performed in each group by comparing the final time point before IFN-α stimulation (end of saline or CQ treatment) with the final time point after IFN-α exposure using paired *t* tests. This approach was selected on the basis of functional analysis indicating that the primary divergence between conditions occurred at later time points. For correlation analyses, simple linear regression was used where appropriate, and statistical significance was assessed using Spearman’s rank correlation test. Data are presented as mean ± SEM unless otherwise indicated. All statistical tests were two-sided, and $P < 0.05$ was considered statistically significant.

Supplementary Material

Refer to Web version on PubMed Central for supplementary material.

Acknowledgments:

We acknowledge the support of the Microscopy Core and the Islet Core of the Indiana Diabetes Research Center (P30DK097512) and of W. Carter for the preparation of iPSC-derived islet cells. Human pancreatic islets and other resources were provided in part by the National Institute of Diabetes and Digestive and Kidney Diseases (NIDDK)–funded IIDP (RRID:SCR _014387) at City of Hope, NIH grant no. U24DK098085. Human islets for research were provided in part by the Alberta Diabetes Institute Islet Core at the University of Alberta in Edmonton (http://bcell.org/adi-isletcore.html) with the assistance of the Human Organ Procurement and Exchange (HOPE) program, Trillium Gift of Life Network (TGLN), and other Canadian organ procurement organizations.

Funding:

Human pancreatic islets and other resources were provided by the NIDDK-funded IIDP (RRID:SCR_014387) at City of Hope, NIH grant no. 2UC4DK098085 and the JDRF-funded IIDP Islet Award Initiative (to A.K.L.). Financial support provided by the Herman B Wells Center to A.K.L. was in part from the Riley Children’s Foundation. Research involving human islet transplants into mice for intravital imaging in the Linnemann laboratory is supported in part by grants from the NIH, R03DK127766 and R01DK124380, to A.K.L. and

using resources and funding provided by the NIDDK-supported Human Islet Research Network (HIRN, RRID: SCR_014393; https://hirnetwork.org) including a HIRN New Investigator Award to A.K.L.

Data, code, and materials availability:

All data associated with this study are present in the paper or the Supplementary Materials. All materials used or generated in this study are commercially available or will be supplied upon reasonable request.

REFERENCES AND NOTES

1. Marasco MR, Linnemann AK, β-cell autophagy in diabetes pathogenesis. Endocrinology 159, 2127–2141 (2018). [PubMed: 29617763]
2. Pearson GL, Gingerich MA, Walker EM, Biden TJ, Soleimanpour SA, A selective look at autophagy in pancreatic β-cells. Diabetes 70, 1229–1241 (2021). [PubMed: 34016598]
3. Mizushima N, Komatsu M, Autophagy: Renovation of cells and tissues. Cell 147, 728–741 (2011). [PubMed: 22078875]
4. Bento CF, Renna M, Ghislat G, Puri C, Ashkenazi A, Vicinanza M, Menzies FM, Rubinsztein DC, Mammalian autophagy: How does it work? Annu. Rev. Biochem. 85, 685–713 (2016). [PubMed: 26865532]
5. Parzych KR, Klionsky DJ, An overview of autophagy: Morphology, mechanism, and regulation. Antioxid. Redox Signal. 20, 460–473 (2014). [PubMed: 23725295]
6. Liu B, Oltvai ZN, Bayir H, Silverman GA, Pak SC, Perlmutter DH, Bahar I, Quantitative assessment of cell fate decision between autophagy and apoptosis. Sci. Rep. 7, 17605 (2017). [PubMed: 29242632]
7. Doherty J, Baehrecke EH, Life, death and autophagy. Nat. Cell Biol. 20, 1110–1117 (2018). [PubMed: 30224761]
8. Lei Y, Klionsky DJ, The emerging roles of autophagy in human diseases. Biomedicines 9, 1651 (2021). [PubMed: 34829881]
9. Yin H, Wu H, Chen Y, Zhang J, Zheng M, Chen G, Li L, Lu Q, The therapeutic and pathogenic role of autophagy in autoimmune diseases. Front. Immunol. 9, 1512 (2018). [PubMed: 30108582]
10. Anding AL, Baehrecke EH, Autophagy in cell life and cell death. Curr. Top. Dev. Biol. 114, 67–91 (2015). [PubMed: 26431564]
11. Mallone R, Halliez C, Rui J, Herold KC, The β-cell in type 1 diabetes pathogenesis: A victim of circumstances or an instigator of tragic events? Diabetes 71, 1603–1610 (2022). [PubMed: 35881836]
12. Atkinson MA, Mirmira RG, The pathogenic “symphony” in type 1 diabetes: A disorder of the immune system, beta cells, and exocrine pancreas. Cell Metab. 35, 1500–1518 (2023). [PubMed: 37478842]
13. Muralidharan C, Conteh AM, Marasco MR, Crowder JJ, Kuipers J, de Boer P, Linnemann AK, Pancreatic beta cell autophagy is impaired in type 1 diabetes. Diabetologia 64, 865–877 (2021). [PubMed: 33515072]
14. Ebato C, Uchida T, Arakawa M, Komatsu M, Ueno T, Komiya K, Azuma K, Hirose T, Tanaka K, Kominami E, Kawamori R, Fujitani Y, Watada H, Autophagy is important in islet homeostasis and compensatory increase of beta cell mass in response to high-fat diet. Cell Metab. 8, 325–332 (2008). [PubMed: 18840363]
15. Aoyagi K, Ohara-Imaizumi M, Itakura M, Torii S, Akimoto Y, Nishiwaki C, Nakamichi Y, Kishimoto T, Kawakami H, Harada A, Takahashi M, Nagamatsu S, VAMP7 regulates autophagy to maintain mitochondrial homeostasis and to control insulin secretion in pancreatic β-cells. Diabetes 65, 1648–1659 (2016). [PubMed: 26953164]
16. Sidarala V, Pearson GL, Parekh VS, Thompson B, Christen L, Gingerich MA, Zhu J, Stromer T, Ren J, Reck EC, Chai B, Corbett JA, Mandrup-Poulsen T, Satin LS, Soleimanpour SA, Mitophagy

protects β cells from inflammatory damage in diabetes. JCI Insight 5, e141138 (2020). [PubMed: 33232298]

17. Klionsky DJ, Abdel-Aziz AK, Abdelfatah S, Abdellatif M, Abdoli A, Abel S, Abeliovich H, Abildgaard MH, Abudu YP, Acevedo-Arozena A, Adamopoulos IE, Adeli K, Adolph TE, Adornetto A, Aflaki E, Agam G, Agarwal A, Aggarwal BB, Agnello M, Agostinis P, Agrewala JN, Agrotis A, Aguilar PV, Ahmad ST, Ahmed ZM, Ahumada-Castro U, Aits S, Aizawa S, Akkoc Y, Akoumianaki T, Akpinar HA, Al-Abd AM, Al-Akra L, Al-Gharaibeh A, Alaoui-Jamali MA, Alberti S, Alcocer-Gómez E, Alessandri C, Ali M, Al-Bari MAA, Aliwaini S, Alizadeh J, Almacellas E, Almasan A, Alonso A, Alonso GD, Altan-Bonnet N, Altieri DC, Álvarez ÉMC, Alves S, da Costa CA, Alzaharna MM, Amadio M, Amantini C, Amaral C, Ambrosio S, Amer AO, Ammanathan V, An Z, Andersen SU, Andrabi SA, Andrade-Silva M, Andres AM, Angelini S, Ann D, Anozie UC, Ansari MY, Antas P, Antebi A, Antón Z, Anwar T, Apetoh L, Apostolova N, Araki T, Araki Y, Arasaki K, Araújo WL, Araya J, Arden C, Arévalo M-A, Arguelles S, Arias E, Arikkath J, Arimoto H, Ariosa AR, Armstrong-James D, Arnauné-Pelloquin L, Aroca A, Arroyo DS, Arsov I, Artero R, Asaro DML, Aschner M, Ashrafizadeh M, Ashur-Fabian O, Atanasov AG, Au AK, Auberger P, Auner HW, Aurelian L, Autelli R, Avagliano L, Ávalos Y, Aveic S, Aveleira CA, Avin-Wittenberg T, Aydin Y, Ayton S, Ayyadevara S, Azzopardi M, Baba M, Backer JM, Backues SK, Bae D-H, Bae O-N, Bae SH, Baehrecke EH, Baek A, Baek S-H, Baek SH, Bagetta G, Bagniewska-Zadworna A, Bai H, Bai J, Bai X, Bai Y, Bairagi N, Baksi S, Balbi T, Baldari CT, Balduini W, Ballabio A, Ballester M, Balazadeh S, Balzan R, Bandopadhyay R, Banerjee S, Banerjee S, Bánréti Á, Bao Y, Baptista MS, Baracca A, Barbati C, Bargiela A, Barilà D, Barlow PG, Barmada SJ, Barreiro E, Barreto GE, Bartek J, Bartel B, Bartolome A, Barve GR, Basagoudanavar SH, Bassham DC, Bast RC Jr., Basu A, Batoko H, Batten I, Baulieu EE, Baumgarner BL, Bayry J, Beale R, Beau I, Beaumatin F, Bechara LRG, Beck GR Jr., Beers MF, Begun J, Behrends C, Behrens GMN, Bei R, Bejarano E, Bel S, Behl C, Belaid A, Belgareh-Touzé N, Bellarosa C, Belleudi F, Pérez MB, Bello-Morales R, de Oliveira Beltran JS, Beltran S, Benbrook DM, Bendorius M, Benitez BA, Benito-Cuesta I, Bensalem J, Berchtold MW, Berezowska S, Bergamaschi D, Bergami M, Bergmann A, Berliocchi L, Berlioz-Torrent C, Bernard A, Berthoux L, Besirli CG, Besteiro S, Betin VM, Beyaert R, Bezbradica JS, Bhaskar K, Bhatia-Kissova I, Bhattacharya R, Bhattacharya S, Bhattacharyya S, Bhuiyan MS, Bhutia SK, Bi L, Bi X, Biden TJ, Bijian K, Billes VA, Binart N, Bincoletto C, Birgisdottir AB, Bjorkoy G, Blanco G, Blas-Garcia A, Blasiak J, Blomgran R, Blomgren K, Blum JS, Boada-Romero E, Boban M, Boesze-Battaglia K, Boeuf P, Boland B, Bomont P, Bonaldo P, Bonam SR, Bonfili L, Bonifacino JS, Boone BA, Bootman MD, Bordi M, Borner C, Bornhauser BC, Borthakur G, Bosch J, Bose S, Botana LM, Botas J, Boulanger CM, Boulton ME, Bourdenx M, Bourgeois B, Bourke NM, Bousquet G, Boya P, Bozhkov PV, Bozi LHM, Bozkurt TO, Brackney DE, Brandts CH, Braun RJ, Braus GH, Bravo-Sagua R, Bravo-San Pedro JM, Brest P, Bringer M-A, Briones-Herrera A, Broaddus VC, Brodersen P, Brodsky JL, Brody SL, Bronson PG, Bronstein JM, Brown CN, Brown RE, Brum PC, Brumell JH, Brunetti-Pierri N, Bruno D, Bryson-Richardson RJ, Bucci C, Buchrieser C, Bueno M, Buitrago-Molina LE, Buraschi S, Buch S, Buchan JR, Buckingham EM, Budak H, Budini M, Bultynck G, Burada F, Burgoyne JR, Burón MI, Bustos V, Büttner S, Butturini E, Byrd A, Cabas I, Cabrera-Benitez S, Cadwell K, Cai J, Cai L, Cai Q, Cairó M, Calbet JA, Caldwell GA, Caldwell KA, Call JA, Calvani R, Calvo AC, Calvo-Rubio Barrera M, Camara NO, Camonis JH, Camougrand N, Campanella M, Campbell EM, Campbell-Valois F-X, Campello S, Campesi I, Campos JC, Camuzard O, Cancino J, de Almeida DC, Canesi L, Caniggia I, Canonico B, Cantí C, Cao B, Caraglia M, Caramés B, Carchman EH, Cardenal-Muñoz E, Cardenas C, Cardenas L, Cardoso SM, Carew JS, Carle GF, Carleton G, Carloni S, Carmona-Gutierrez D, Carneiro LA, Carnevali O, Carosi JM, Carra S, Carrier A, Carrier L, Carroll B, Carter AB, Carvalho AN, Casanova M, Casas C, Casas J, Cassioli C, Castillo EF, Castillo K, Castillo-Lluva S, Castoldi F, Castori M, Castro AF, Castro-Caldas M, Castro-Hernandez J, Castro-Obregon S, Catz SD, Cavadas C, Cavaliere F, Cavallini G, Cavinato M, Cayuela ML, Rica PC, Cecarini V, Cecconi F, Cechowska-Pasko M, Cenci S, Ceperuelo-Mallafré V, Cerqueira JJ, Cerutti JM, Cervia D, Cetintas VB, Cetrullo S, Chae H-J, Chagin AS, Chai C-Y, Chakrabarti G, Chakrabarti O, Chakraborty T, Chakraborty T, Chami M, Chamilos G, Chan DW, Chan EYW, Chan ED, Chan HYE, Chan HH, Chan H, Chan MTV, Chan YS, Chandra PK, Chang C-P, Chang C, Chang H-C, Chang K, Chao J, Chapman T, Charlet-Berguerand N, Chatterjee S, Chaube SK, Chaudhary A, Chauhan S, Chaum E, Checler F, Cheetham ME, Chen C-S, Chen G-C, Chen J-F, Chen LL, Chen

L, Chen L, Chen M, Chen M-K, Chen N, Chen Q, Chen R-H, Chen S, Chen W, Chen W, Chen X-M, Chen X-W, Chen X, Chen Y, Chen Y-G, Chen Y, Chen Y, Chen Y-J, Chen Y-Q, Chen ZS, Chen Z, Chen Z-H, Chen ZJ, Chen Z, Cheng H, Cheng J, Cheng S-Y, Cheng W, Cheng X, Cheng X-T, Cheng Y, Cheng Z, Chen Z, Cheong H, Cheong JK, Chernyak BV, Cherry S, Cheung CFR, Cheung CHA, Cheung K-H, Chevet E, Chi RJ, Chiang AKS, Chiaradonna F, Chiarelli R, Chiariello M, Chica N, Chiocca S, Chiong M, Chiou S-H, Chiramel AI, Chiurchiù V, Cho D-H, Choe S-K, Choi AMK, Choi ME, Choudhury KR, Chow NS, Chu CT, Chua JP, Chua JJE, Chung H, Chung KP, Chung S, Chung S-H, Chung Y-L, Cianfanelli V, Ciechomska IA, Cifuentes M, Cinque L, Cirak S, Cirone M, Clague MJ, Clarke R, Clementi E, Coccia EM, Codogno P, Cohen E, Cohen MM, Colasanti T, Colasuonno F, Colbert RA, Colell A, Čolić M, Coll NS, Collins MO, Colombo MI, Colón-Ramos DA, Combaret L, Comincini S, Cominetti MR, Consiglio A, Conte A, Conti F, Contu VR, Cookson MR, Coombs KM, Coppens I, Corasaniti MT, Corkery DP, Cordes N, Cortese K, do Carmo Costa M, Costantino S, Costelli P, Coto-Montes A, Crack PJ, Crespo JL, Criollo A, Crippa V, Cristofani R, Csizmadia T, Cuadrado A, Cui B, Cui J, Cui Y, Cui Y, Culetto E, Cumino AC, Cybulsky AV, Czaja MJ, Czuczwar SJ, D'Adamo S, D'Amelio M, D'Arcangelo D, D'Lugos AC, D'Orazi G, da Silva JA, Dafsari HS, Dagda RK, Dagdas Y, Daglia M, Dai X, Dai Y, Dai Y, Col JD, Dalhaimer P, Valle LD, Dallenga T, Dalmasso G, Damme M, Dando I, Dantuma NP, Darling AL, Das H, Dasarathy S, Dasari SK, Dash S, Daumke O, Dauphinee AN, Davies JS, Dávila VA, Davis RJ, Davis T, Naidu SD, De Amicis F, De Bosscher K, De Felice F, De Franceschi L, De Leonibus C, de Mattos Barbosa MG, De Meyer GRY, De Milito A, De Nunzio C, De Palma C, De Santi M, De Virgilio C, De Zio D, Debnath J, De Bosch BJ, Decuypere J-P, Deehan MA, Deflorian G, De Gregori J, Dehay B, Rio GD, Delaney JR, Delbridge LMD, Delorme-Axford E, Delpino MV, Demarchi F, Dembitz V, Demers ND, Deng H, Deng Z, Dengjel J, Dent P, Denton D, De Pamphilis ML, Der CJ, Deretic V, Descoteaux A, Devis L, Devkota S, Devuyst O, Dewson G, Dharmasivam M, Dhiman R, di Bernardo D, Cristina MD, Domenico FD, Fazio PD, Fonzo AD, Guardo GD, Di Guglielmo GM, Leo LD, Malta CD, Nardo AD, Rienzo MD, Sano FD, Diallinas G, Diao J, Diaz-Araya G, Díaz-Laviada I, Dickinson JM, Diederich M, Dieudé M, Dikic I, Ding S, Ding W-X, Dini L, Dinić J, Dinic M, Dinkova-Kostova AT, Dionne MS, Distler JHW, Diwan A, Dixon IMC, Djavaheri-Mergny M, Dobrinski I, Dobrovinskaya O, Dobrowolski R, Dobson RCJ, Đokić J, Emre SD, Donadelli M, Dong B, Dong X, Dong Z, Ii GWD, Dotsch V, Dou H, Dou J, Dowaidar M, Dridi S, Drucker L, Du A, Du C, Du G, Du H-N, Du L-L, du Toit A, Duan S-B, Duan X, Duarte SP, Dubrovska A, Dunlop EA, Dupont N, Durán RV, Dwarakanath BS, Dyshlovoy SA, Ebrahimi-Fakhari D, Eckhart L, Edelstein CL, Efferth T, Eftekharpour E, Eichinger L, Eid N, Eisenberg T, Eissa NT, Eissa S, Ejarque M, Andaloussi AE, El-Hage N, El-Naggar S, Eleuteri AM, El-Shafey ES, Elgendy M, Eliopoulos AG, Elizalde MM, Elks PM, Elsasser H-P, Elsherbiny ES, Emerling BM, Emre NCT, Eng CH, Engedal N, Engelbrecht A-M, Engelsen AST, Enserink JM, Escalante R, Esclatine A, Escobar-Henriques M, Eskelinen E-L, Espert L, Eusebio M-O, Fabrias G, Fabrizi C, Facchiano A, Facchiano F, Fadeel B, Fader C, Faesen AC, Fairlie WD, Falcó A, Falkenburger BH, Fan D, Fan J, Fan Y, Fang EF, Fang Y, Fang Y, Fanto M, Farfel-Becker T, Faure M, Fazeli G, Fedele AO, Feldman AM, Feng D, Feng J, Feng L, Feng Y, Feng Y, Feng W, Araujo TF, Ferguson TA, Fernández ÁF, Fernandez-Checa JC, Fernández-Veledo S, Fernie AR, Ferrante AW Jr., Ferraresi A, Ferrari MF, Ferreira JCB, Ferro-Novick S, Figueras A, Filadi R, Filigheddu N, Filippi-Chiela E, Filomeni G, Fimia GM, Fineschi V, Finetti F, Finkbeiner S, Fisher EA, Fisher PB, Flamigni F, Fliesler SJ, Flo TH, Florance I, Florey O, Florio T, Fodor E, Follo C, Fon EA, Forlino A, Fornai F, Fortini P, Fracassi A, Fraldi A, Franco B, Franco R, Franconi F, Frankel LB, Friedman SL, Fröhlich LF, Frühbeck G, Fuentes JM, Fujiki Y, Fujita N, Fujiwara Y, Fukuda M, Fulda S, Furic L, Furuya N, Fusco C, Gack MU, Gaffke L, Galadari S, Galasso A, Galindo MF, Kankanamalage SG, Galluzzi L, Galy V, Gammoh N, Gan B, Ganley IG, Gao F, Gao H, Gao M, Gao P, Gao S-J, Gao W, Gao X, Garcera A, Garcia MN, Garcia VE, García-Del Portillo F, Garcia-Escudero V, Garcia-Garcia A, Garcia-Macia M, García-Moreno D, Garcia-Ruiz C, García-Sanz P, Garg AD, Gargini R, Garofalo T, Garry RF, Gassen NC, Gatica D, Ge L, Ge W, Geiss-Friedlander R, Gelfi C, Genschik P, Gentle IE, Gerbino V, Gerhardt C, Germain K, Germain M, Gewirtz DA, Afshar EG, Ghavami S, Ghigo A, Ghosh M, Giamas G, Giampietri C, Giatromanolaki A, Gibson GE, Gibson SB, Ginet V, Giniger E, Giorgi C, Girao H, Girardin SE, Giridharan M, Giuliano S, Giulivi C, Giuriato S, Giustiniani J, Gluschko A, Goder V, Goginashvili A, Golab J, Goldstone DC, Golebiewska A, Gomes LR, Gomez R, Gómez-Sánchez R, Gomez-Puerto MC, Gomez-Sintes R, Gong Q, Goni FM, González-Gallego J, Gonzalez-

Hernandez T, Gonzalez-Polo RA, Gonzalez-Reyes JA, González-Rodríguez P, Goping IS, Gorbatyuk MS, Gorbunov NV, Görgülü K, Gorojod RM, Gorski SM, Goruppi S, Gotor C, Gottlieb RA, Gozes I, Gozuacik D, Graef M, Gräler MH, Granatiero V, Grasso D, Gray JP, Green DR, Greenhough A, Gregory SL, Griffin EF, Grinstaff MW, Gros F, Grose C, Gross AS, Gruber F, Grumati P, Grune T, Gu X, Guan J-L, Guardia CM, Guda K, Guerra F, Guerri C, Guha P, Guillén C, Gujar S, Gukovskaya A, Gukovsky I, Gunst J, Günther A, Guntur AR, Guo C, Guo C, Guo H, Guo L-W, Guo M, Gupta P, Gupta SK, Gupta S, Gupta VB, Gupta V, Gustafsson AB, Gutterman DD, Ranjitha HB, Haapasalo A, Haber JE, Hać A, Hadano S, Hafrén AJ, Haidar M, Hall BS, Halldén G, Hamacher-Brady A, Hamann A, Hamasaki M, Han W, Hansen M, Hanson PI, Hao Z, Harada M, Harhaji-Trajkovic L, Hariharan N, Haroon N, Harris J, Hasegawa T, Nagoor NH, Haspel JA, Haucke V, Hawkins WD, Hay BA, Haynes CM, Hayrabedyan SB, Hays TS, He C, He Q, He R-R, He Y-W, He Y-Y, Heakal Y, Heberle AM, Hejtmancik JF, Helgason GV, Henkel V, Herb M, Hergovich A, Herman-Antosiewicz A, Hernández A, Hernandez C, Hernandez-Diaz S, Hernandez-Gea V, Herpin A, Herreros J, Hervás JH, Hesselson D, Hetz C, Heussler VT, Higuchi Y, Hilfiker S, Hill JA, Hlavacek WS, Ho EA, Ho IHT, Ho PW-L, Ho S-L, Ho WY, Hobbs GA, Hochstrasser M, Hoet PHM, Hofius D, Hofman P, Höhn A, Holmberg CI, Hombrebueno JR, Hong C-WHY-R, Hooper LV, Hoppe T, Horos R, Hoshida Y, Hsin I-L, Hsu H-Y, Hu B, Hu D, Hu L-F, Hu MC, Hu R, Hu W, Hu Y-C, Hu Z-W, Hua F, Hua J, Hua Y, Huan C, Huang C, Huang C, Huang C, Huang C, Huang H, Huang K, Huang MLH, Huang R, Huang S, Huang T, Huang X, Huang YJ, Huber TB, Hubert V, Hubner CA, Hughes SM, Hughes WE, Humbert M, Hummer G, Hurley JH, Hussain S, Hussain S, Hussey PJ, Hutabarat M, Hwang H-Y, Hwang S, Ieni A, Ikeda F, Imagawa Y, Imai Y, Imbriano C, Imoto M, Inman DM, Inoki K, Iovanna J, Iozzo RV, Ippolito G, Irazoqui JE, Iribarren P, Ishaq M, Ishikawa M, Ishimwe N, Isidoro C, Ismail N, Issazadeh-Navikas S, Itakura E, Ito D, Ivankovic D, Ivanova S, Iyer AKV, Izquierdo JM, Izumi M, Jäättelä M, Jabir MS, Jackson WT, Jacobo-Herrera N, Jacomin A-C, Jacquin E, Jadiya P, Jaeschke H, Jagannath C, Jakobi AJ, Jakobsson J, Janji B, Jansen-Dürr P, Jansson PJ, Jantsch J, Januszewski S, Jassey A, Jean S, Jeltsch-David H, Jendelova P, Jenny A, Jensen TE, Jessen N, Jewell JL, Ji J, Jia L, Jia R, Jiang L, Jiang Q, Jiang R, Jiang T, Jiang X, Jiang Y, Jimenez-Sanchez M, Jin E-J, Jin F, Jin H, Jin L, Jin L, Jin M, Jin S, Jo E-K, Joffre C, Johansen T, Johnson GVW, Johnston SA, Jokitalo E, Jolly MK, Joosten LAB, Jordan J, Joseph B, Ju D, Ju J-S, Ju J, Juárez E, Judith D, Juhász G, Jun Y, Jung CH, Jung S-C, Jung YK, Jungbluth H, Jungverdorben J, Just S, Kaarniranta K, Kaasik A, Kabuta T, Kaganovich D, Kahana A, Kain R, Kajimura S, Kalamvoki M, Kalia M, Kalinowski DS, Kaludercic N, Kalvari I, Kaminska J, Kaminskyy VO, Kanamori H, Kanasaki K, Kang C, Kang R, Kang SS, Kaniyappan S, Kanki T, Kanneganti T-D, Kanthasamy AG, Kanthasamy A, Kantorow M, Kapuy O, Karamouzis MV, Karim MR, Karmakar P, Katare RG, Kato M, Kaufmann SHE, Kauppinen A, Kaushal GP, Kaushik S, Kawasaki K, Kazan K, Ke P-Y, Keating DJ, Keber U, Kehrl JH, Keller KE, Keller CW, Kemper JK, Kenific CM, Kepp O, Kermorgant S, Kern A, Ketteler R, Keulers TG, Khalfin B, Khalil H, Khambu B, Khan SY, Khandelwal VKM, Khandia R, Kho W, Khobrekar NV, Khuansuwan S, Khundadze M, Killackey SA, Kim D, Kim DR, Kim D-H, Kim D-E, Kim EY, Kim E-K, Kim H-R, Kim H-S, Kim H-R, Kim JH, Kim JK, Kim J-H, Kim J, Kim JH, Kim KI, Kim PK, Kim S-J, Kimball SR, Kimchi A, Kimmelman AC, Kimura T, King MA, Kinghorn KJ, Kinsey CG, Kirkin V, Kirshenbaum LA, Kiselev SL, Kishi S, Kitamoto K, Kitaoka Y, Kitazato K, Kitsis RN, Kittler JT, Kjaerulff O, Klein PS, Klopstock T, Klucken J, Knævelsrud H, Knorr RL, Ko BCB, Ko F, Ko J-L, Kobayashi H, Kobayashi S, Koch I, Koch JC, Koenig U, Kögel D, Koh YH, Koike M, Kohlwein SD, Kocaturk NM, Komatsu M, König J, Kono T, Kopp BT, Korcsmaros T, Korkmaz G, Korolchuk VI, Korsnes MS, Koskela A, Kota J, Kotake Y, Kotler ML, Kou Y, Koukourakis MI, Koustas E, Kovacs AL, Kovács T, Koya D, Kozako T, Kraft C, Krainc D, Krämer H, Krasnodembskaya AD, Kretz-Remy C, Kroemer G, Ktistakis NT, Kuchitsu K, Kuenen S, Kuerschner L, Kukar T, Kumar A, Kumar A, Kumar D, Kumar D, Kumar S, Kume S, Kumsta C, Kundu CN, Kundu M, Kunnumakkara AB, Kurgan L, Kutateladze TG, Kutlu O, Kwak SA, Kwon HJ, Kwon TK, Kwon YT, Kyrmizi I, Spada AL, Labonté P, Ladoire S, Laface I, Lafont F, Lagace DC, Lahiri V, Lai Z, Laird AS, Lakkaraju A, Lamark T, Lan S-H, Landajuela A, Lane DJR, Lane JD, Lang CH, Lange C, Langel Ü, Langer R, Lapaquette P, Laporte J, La Russo NF, Lastres-Becker I, Lau WCY, Laurie GW, Lavandero S, Law BYK, Law HK-W, Layfield R, Le W, Stunff HL, Leary AY, Lebrun J-J, Leck LYW, Leduc-Gaudet J-P, Lee C, Lee C-P, Lee D-H, Lee EB, Lee EF, Lee GM, Lee H-J, Lee HK, Lee JM, Lee JS, Lee J-A, Lee J-Y, Lee JH, Lee M, Lee MG, Lee MJ, Lee M-S, Lee SY, Lee S-J, Lee SY, Lee SB, Lee WH, Lee Y-R, Lee Y-H, Lee Y,

Lefebvre C, Legouis R, Lei YL, Lei Y, Leikin S, Leitinger G, Lemus L, Leng S, Lenoir O, Lenz G, Lenz HJ, Lenzi P, León Y, Leopoldino AM, Leschczyk C, Leskelä S, Letellier E, Leung C-T, Leung PS, Leventhal JS, Levine B, Lewis PA, Ley K, Li B, Li D-Q, Li J, Li J, Li J, Li K, Li L, Li M, Li M, Li M, Li M, Li M, Li P-L, Li M-Q, Li Q, Li S, Li T, Li W, Li W, Li X, Li Y-P, Li Y, Li Z, Li Z, Li Z, Lian J, Liang C, Liang Q, Liang W, Liang Y, Liang YT, Liao G, Liao L, Liao M, Liao Y-F, Librizzi M, Lie PPY, Lilly MA, Lim HJ, Lima TRR, Limana F, Lin C, Lin C-W, Lin D-S, Lin F-C, Lin JD, Lin KM, Lin K-H, Lin L-T, Lin P-H, Lin Q, Lin S, Lin S-J, Lin W, Lin X, Lin Y-X, Lin Y-S, Linden R, Lindner P, Ling S-C, Lingor P, Linnemann AK, Liou Y-C, Lipinski MM, Lipovšek S, Lira VA, Lisiak N, Liton PB, Liu C, Liu C-H, Liu C-F, Liu CH, Liu F, Liu H, Liu H-S, Liu H-F, Liu H, Liu J, Liu J, Liu J, Liu L, Liu L, Liu M, Liu Q, Liu W, Liu W, Liu X-H, Liu X, Liu X, Liu X, Liu X, Liu Y, Liu Y, Liu Y, Liu Y, Liu Y, Livingston JA, Lizard G, Lizcano JM, Ljubojevic-Holzer S, LLeonart ME, Llobet-Navàs D, Llorente A, Lo CH, Lobato-Márquez D, Long Q, Long YC, Loos B, Loos JA, López MG, López-Doménech G, López-Guerrero JA, López-Jiménez AT, López-Pérez Ó, López-Valero I, Lorenowicz MJ, Lorente M, Lorincz P, Lossi L, Lotersztajn S, Lovat PE, Lovell JF, Lovy A, Lőw P, Lu G, Lu H, Lu J-H, Lu J-J, Lu M, Lu S, Luciani A, Lucocq JM, Ludovico P, Luftig MA, Luhr M, Luis-Ravelo D, Lum JJ, Luna-Dulcey L, Lund AH, Lund VK, Lünemann JD, Lüningschrör P, Luo H, Luo R, Luo S, Luo Z, Luparello C, Lüscher B, Luu L, Lyakhovich A, Lyamzaev KG, Lystad AH, Lytvynchuk L, Ma AC, Ma C, Ma M, Ma N-F, Ma Q-H, Ma X, Ma Y, Ma Z, MacDougald OA, Macian F, MacIntosh GC, MacKeigan JP, Macleod KF, Maday S, Madeo F, Madesh M, Madl T, Madrigal-Matute J, Maeda A, Maejima Y, Magarinos M, Mahavadi P, Maiani E, Maiese K, Maiti P, Maiuri MC, Majello B, Major MB, Makareeva E, Malik F, Mallilankaraman K, Malorni W, Maloyan A, Mammadova N, Man GCW, Manai F, Mancias JD, Mandelkow E-M, Mandell MA, Manfredi AA, Manjili MH, Manjithaya R, Manque P, Manshian BB, Manzano R, Manzoni C, Mao K, Marchese C, Marchetti S, Marconi AM, Marcucci F, Mardente S, Mareninova OA, Margeta M, Mari M, Marinelli S, Marinelli O, Mariño G, Mariotto S, Marshall RS, Marten MR, Martens S, Martin APJ, Martin KR, Martin S, Martin S, Martín-Segura A, Martín-Acebes MA, Martin-Burriel I, Martin-Rincon M, Martin-Sanz P, Martina JA, Martinet W, Martinez A, Martinez A, Martinez J, Velazquez MM, Martinez-Lopez N, Martinez-Vicente M, Martins DO, Martins JO, Martins WK, Martins-Marques T, Marzetti E, Masaldan S, Masclaux-Daubresse C, Mashek DG, Massa V, Massieu L, Masson GR, Masuelli L, Masyuk AI, Masyuk TV, Matarrese P, Matheu A, Matoba S, Matsuzaki S, Mattar P, Matte A, Mattoscio D, Mauriz JL, Mauthe M, Mauvezin C, Maverakis E, Maycotte P, Mayer J, Mazzoccoli G, Mazzoni C, Mazzulli JR, Carty NM, Donald CM, Gill MRM, McKenna SL, McLaughlin BA, Loughlin FM, Niven MAM, McWilliams TG, Mechta-Grigoriou F, Medeiros TC, Medina DL, Megeney LA, Megyeri K, Mehrpour M, Mehta JL, Meijer AJ, Meijer AH, Mejlvang J, Meléndez A, Melk A, Memisoglu G, Mendes AF, Meng D, Meng F, Meng T, Menna-Barreto R, Menon MB, Mercer C, Mercier AE, Mergny J-L, Merighi A, Merkley SD, Merla G, Meske V, Mestre AC, Metur SP, Meyer C, Meyer H, Mi W, Mialet-Perez J, Miao J, Micale L, Miki Y, Milan E, Milczarek M, Miller DL, Miller SI, Miller S, Millward SW, Milosevic I, Minina EA, Mirzaei H, Mirzaei HR, Mirzaei M, Mishra A, Mishra N, Mishra PK, Marjanovic MM, Misasi R, Misra A, Misso G, Mitchell C, Mitou G, Miura T, Miyamoto S, Miyazaki M, Miyazaki M, Miyazaki T, Miyazawa K, Mizushima N, Mogensen TH, Mograbi B, Mohammadinejad R, Mohamud Y, Mohanty A, Mohapatra S, Möhlmann T, Mohmmed A, Moles A, Moley KH, Molinari M, Mollace V, Møller AB, Mollereau B, Mollinedo F, Montagna C, Monteiro MJ, Montella A, Montes LR, Montico B, Mony VK, Compagnoni GM, Moore MN, Moosavi MA, Mora AL, Mora M, Morales-Alamo D, Moratalla R, Moreira PI, Morelli E, Moreno S, Moreno-Blas D, Moresi V, Morga B, Morgan AH, Morin F, Morishita H, Moritz OL, Moriyama M, Moriyasu Y, Morleo M, Morselli E, Moruno-Manchon JF, Moscat J, Mostowy S, Motori E, Moura AF, Moustaid-Moussa N, Mrakovcic M, Muciño-Hernández G, Mukherjee A, Mukhopadhyay S, Levy JMM, Mulero V, Muller S, Münch C, Munjal A, Munoz-Canoves P, Muñoz-Galdeano T, Münz C, Murakawa T, Muratori C, Murphy BM, Murphy JP, Murthy A, Myöhänen TT, Mysorekar IU, Mytych J, Nabavi SM, Nabissi M, Nagy P, Nah J, Nahimana A, Nakagawa I, Nakamura K, Nakatogawa H, Nandi SS, Nanjundan M, Nanni M, Napolitano G, Nardacci R, Narita M, Nassif M, Nathan I, Natsumeda M, Naude RJ, Naumann C, Naveiras O, Navid F, Nawrocki ST, Nazarko TY, Nazio F, Negoita F, Neill T, Neisch AL, Neri LM, Netea MG, Neubert P, Neufeld TP, Neumann D, Neutzner A, Newton PT, Ney PA, Nezis IP, Ng CCW, Ng TB, Nguyen HTT, Nguyen LT, Ni H-M, Cheallaigh CN, Ni Z, Nicolao MC, Nicoli F, Nieto-Diaz M, Nilsson P, Ning S, Niranjan R, Nishimune H,

Niso-Santano M, Nixon RA, Nobili A, Nobrega C, Noda T, Nogueira-Recalde U, Nolan TM, Nombela I, Novak I, Novoa B, Nozawa T, Nukina N, Nussbaum-Krammer C, Nylandsted J, O'Donovan TR, O'Leary SM, O'Rourke EJ, O'Sullivan MP, O'Sullivan TE, Oddo S, Oehme I, Ogawa M, Ogier-Denis E, Ogmundsdottir MH, Ogretmen B, Oh GT, Oh S-H, Oh YJ, Ohama T, Ohashi Y, Ohmuraya M, Oikonomou V, Ojha R, Okamoto K, Okazawa H, Oku M, Oliván S, Oliveira JMA, Ollmann M, Olzmann JA, Omari S, Omary MB, Önal G, Ondrej M, Ong S-B, Ong S-G, Onnis A, Orellana JA, Orellana-Muñoz S, Del Mar Ortega-Villaizan M, Ortiz-Gonzalez XR, Ortona E, Osiewacz HD, Osman A-HK, Osta R, Otegui MS, Otsu K, Ott C, Ottobrini L, Ou J-HJ, Outeiro TF, Oynebraten I, Ozturk M, Pagès G, Pahari S, Pajares M, Pajvani UB, Pal R, Paladino S, Pallet N, Palmieri M, Palmisano G, Palumbo C, Pampaloni F, Pan L, Pan Q, Pan W, Pan X, Panasyuk G, Pandey R, Pandey UB, Pandya V, Paneni F, Pang SY, Panzarini E, Papademetrio DL, Papaleo E, Papinski D, Papp D, Park EC, Park HT, Park J-M, Park J-I, Park JT, Park J, Park SC, Park S-Y, Parola AH, Parys JB, Pasquier A, Pasquier B, Passos JF, Pastore N, Patel HH, Patschan D, Pattingre S, Pedraza-Alva G, Pedraza-Chaverri J, Pedrozo Z, Pei G, Pei J, Peled-Zehavi H, Pellegrini JM, Pelletier J, Peñalva MA, Peng D, Peng Y, Penna F, Pennuto M, Pentimalli F, Pereira CM, Pereira GJS, Pereira LC, de Almeida LP, Perera ND, Pérez-Lara Á, Perez-Oliva AB, Pérez-Pérez ME, Periyasamy P, Perl A, Perrotta C, Perrotta I, Pestell RG, Petersen M, Petrache I, Petrovski G, Pfirrmann T, Pfister AS, Philips JA, Pi H, Picca A, Pickrell AM, Picot S, Pierantoni GM, Pierdominici M, Pierre P, Pierrefite-Carle V, Pierzynowska K, Pietrocola F, Pietruczuk M, Pignata C, Pimentel-Muiños FX, Pinar M, Pinheiro RO, Pinkas-Kramarski R, Pinton P, Pircs K, Piya S, Pizzo P, Plantinga TS, Platta HW, Plaza-Zabala A, Plomann M, Plotnikov EY, Plun-Favreau H, Pluta R, Pocock R, Pöggeler S, Pohl C, Poirot M, Poletti A, Ponpuak M, Popelka H, Popova B, Porta H, Alcon SP, Portilla-Fernandez E, Post M, Potts MB, Poulton J, Powers T, Prahlad V, Prajsnar TK, Praticò D, Prencipe R, Priault M, Proikas-Cezanne T, Promponas VJ, Proud CG, Puertollano R, Puglielli L, Pulinilkunnil T, Puri D, Puri R, Puyal J, Qi X, Qi Y, Qian W, Qiang L, Qiu Y, Quadrilatero J, Quarleri J, Raben N, Rabinowich H, Ragona D, Ragusa MJ, Rahimi N, Rahmati M, Raia V, Raimundo N, Rajasekaran N-S, Rao SR, Rami A, Ramírez-Pardo I, Ramsden DB, Randow F, Rangarajan PN, Ranieri D, Rao H, Rao L, Rao R, Rathore S, Ratnayaka JA, Ratovitski EA, Ravanan P, Ravegnini G, Ray SK, Razani B, Rebecca V, Reggiori F, Régnier-Vigouroux A, Reichert AS, Reigada D, Reiling JH, Rein T, Reipert S, Rekha RS, Ren H, Ren J, Ren W, Renault T, Renga G, Reue K, Rewitz K, de Andrade Ramos BR, Riazuddin SA, Ribeiro-Rodrigues TM, Ricci J-E, Ricci R, Riccio V, Richardson DR, Rikihisa Y, Risbud MV, Risueño RM, Ritis K, Rizza S, Rizzuto R, Roberts HC, Roberts LD, Robinson KJ, Roccheri MC, Rocchi S, Rodney GG, Rodrigues T, Rodrigues Silva VR, Rodriguez A, Rodriguez-Barrueco R, Rodriguez-Henche N, Rodriguez-Rocha H, Roelofs J, Rogers RS, Rogov VV, Rojo AI, Rolka K, Romanello V, Romani L, Romano A, Romano PS, Romeo-Guitart D, Romero LC, Romero M, Roney JC, Rongo C, Roperto S, Rosenfeldt MT, Rosenstiel P, Rosenwald AG, Roth KA, Roth L, Roth S, Rouschop KMA, Roussel BD, Roux S, Rovere-Querini P, Roy A, Rozieres A, Ruano D, Rubinsztein DC, Rubtsova MP, Ruckdeschel K, Ruckenstuhl C, Rudolf E, Rudolf R, Ruggieri A, Ruparelia AA, Rusmini P, Russell RR, Russo GL, Russo M, Russo R, Ryabaya OO, Ryan KM, Ryu K-Y, Sabater-Arcis M, Sachdev U, Sacher M, Sachse C, Sadhu A, Sadoshima J, Safren N, Saftig P, Sagona AP, Sahay G, Sahebkar A, Sahin M, Sahin O, Sahni S, Saito N, Saito S, Saito T, Sakai R, Sakai Y, Sakamaki J-I, Saksela K, Salazar G, Salazar-Degracia A, Salekdeh GH, Saluja AK, Sampaio-Marques B, Sanchez MC, Sanchez-Alcazar JA, Sanchez-Vera V, Sancho-Shimizu V, Sanderson JT, Sandri M, Santaguida S, Santambrogio L, Santana MM, Santoni G, Sanz A, Sanz P, Saran S, Sardiello M, Sargeant TJ, Sarin A, Sarkar C, Sarkar S, Sarrias M-R, Sarkar S, Sarmah DT, Sarparanta J, Sathyanarayan A, Sathyanarayanan R, Scaglione KM, Scatozza F, Schaefer L, Schafer ZT, Schaible UE, Schapira AHV, Scharl M, Schatzl HM, Schein CH, Scheper W, Scheuring D, Schiaffino MV, Schiappacassi M, Schindl R, Schlattner U, Schmidt O, Schmitt R, Schmidt SD, Schmitz I, Schmukler E, Schneider A, Schneider BE, Schober R, Schoijet AC, Schott MB, Schramm M, Schröder B, Schuh K, Schüller C, Schulze RJ, Schürmanns L, Schwamborn JC, Schwarten M, Scialo F, Sciarretta S, Scott MJ, Scotto KW, Scovassi AI, Scrima A, Scrivo A, Sebastian D, Sebti S, Sedej S, Segatori L, Segev N, Seglen PO, Seiliez I, Seki E, Selleck SB, Sellke FW, Selsby JT, Sendtner M, Senturk S, Seranova E, Sergi C, Serra-Moreno R, Sesaki H, Settembre C, Setty SRG, Sgarbi G, Sha O, Shacka JJ, Shah JA, Shang D, Shao C, Shao F, Sharbati S, Sharkey LM, Sharma D, Sharma G, Sharma K, Sharma P, Sharma S, Shen H-M, Shen H, Shen J, Shen M, Shen W, Shen Z, Sheng R, Sheng Z, Sheng Z-H, Shi J, Shi X, Shi Y-H, Shiba-

Fukushima K, Shieh J-J, Shimada Y, Shimizu S, Shimozawa M, Shintani T, Shoemaker CJ, Shojaei S, Shoji I, Shravage BV, Shridhar V, Shu C-W, Shu H-B, Shui K, Shukla AK, Shutt TE, Sica V, Siddiqui A, Sierra A, Sierra-Torre V, Signorelli S, Sil P, de Andrade Silva BJ, Silva JD, Silva-Pavez E, Silvente-Poirot S, Simmonds RE, Simon AK, Simon H-U, Simons M, Singh A, Singh LP, Singh R, Singh SV, Singh SK, Singh SB, Singh S, Singh SP, Sinha D, Sinha RA, Sinha S, Sirko A, Sirohi K, Sivridis EL, Skendros P, Skirycz A, Slaninová I, Smaili SS, Smertenko A, Smith MD, Soenen SJ, Sohn EJ, Sok SPM, Solaini G, Soldati T, Soleimanpour SA, Soler RM, Solovchenko A, Somarelli JA, Sonawane A, Song F, Song HK, Song J-X, Song K, Song Z, Soria LR, Sorice M, Soukas AA, Soukup S-F, Sousa D, Sousa N, Spagnuolo PA, Spector SA, Bharath MMS, Clair DS, Stagni V, Staiano L, Stalnecker CA, Stankov MV, Stathopulos PB, Stefan K, Stefan SM, Stefanis L, Steffan JS, Steinkasserer A, Stenmark H, Sterneckert J, Stevens C, Stoka V, Storch S, Stork B, Strappazzon F, Strohecker AM, Stupack DG, Su H, Su L-Y, Su L, Suarez-Fontes AM, Subauste CS, Subbian S, Subirada PV, Sudhandiran G, Sue CM, Sui X, Summers C, Sun G, Sun J, Sun K, Sun M-X, Sun Q, Sun Y, Sun Z, Sunahara KKS, Sundberg E, Susztak K, Sutovsky P, Suzuki H, Sweeney G, Symons JD, Sze SCW, Szewczyk NJ, Tabęcka-Łonczynska A, Tabolacci C, Tacke F, Taegtmeyer H, Tafani M, Tagaya M, Tai H, Tait SWG, Takahashi Y, Takats S, Talwar P, Tam C, Tam SY, Tampellini D, Tamura A, Tan CT, Tan E-K, Tan Y-Q, Tanaka M, Tanaka M, Tang D, Tang J, Tang T-S, Tanida I, Tao Z, Taouis M, Tatenhorst L, Tavernarakis N, Taylor A, Taylor GA, Taylor JM, Tchetina E, Tee AR, Tegeder I, Teis D, Teixeira N, Teixeira-Clerc F, Tekirdag KA, Tencomnao T, Tenreiro S, Tepikin AV, Testillano PS, Tettamanti G, Tharaux P-L, Thedieck K, Thekkinghat AA, Thellung S, Thinwa JW, Thirumalaikumar VP, Thomas SM, Thomes PG, Thorburn A, Thukral L, Thum T, Thumm M, Tian L, Tichy A, Till A, Timmerman V, Titorenko VI, Todi SV, Todorova K, Toivonen JM, Tomaipitinca L, Tomar D, Tomas-Zapico C, Tomić S, Tong BC-K, Tong C, Tong X, Tooze SA, Torgersen ML, Torii S, Torres-López L, Torriglia A, Towers CG, Towns R, Toyokuni S, Trajkovic V, Tramontano D, Tran Q-G, Travassos LH, Trelford CB, Tremel S, Trougakos IP, Tsao BP, Tschan MP, Tse H-F, Tse TF, Tsugawa H, Tsvetkov AS, Tumbarello DA, Tumtas Y, Tuñón MJ, Turcotte S, Turk B, Turk V, Turner BJ, Tuxworth RI, Tyler JK, Tyutereva EV, Uchiyama Y, Ugun-Klusek A, Uhlig HH, Ułamek-Kozioł M, Ulasov IV, Umekawa M, Ungermann C, Unno R, Urbe S, Uribe-Carretero E, Üstün S, Uversky VN, Vaccari T, Vaccaro MI, Vahsen BF, Vakifahmetoglu-Norberg H, Valdor R, Valente MJ, Valko A, Vallee RB, Valverde AM, Van den Berghe G, van der Veen S, Van Kaer L, van Loosdregt J, van Wijk SJL, Vandenberghe W, Vanhorebeek I, Vannier-Santos MA, Vannini N, Vanrell MC, Vantaggiato C, Varano G, Varela-Nieto I, Varga M, Vasconcelos MH, Vats S, Vavvas DG, Vega-Naredo I, Vega-Rubin-de-Celis S, Velasco G, Velázquez AP, Vellai T, Vellenga E, Velotti F, Verdier M, Verginis P, Vergne I, Verkade P, Verma M, Verstreken P, Vervliet T, Vervoorts J, Vessoni AT, Victor VM, Vidal M, Vidoni C, Vieira OV, Vierstra RD, Viganó S, Vihinen H, Vijayan V, Vila M, Vilar M, Villalba JM, Villalobo A, Villarejo-Zori B, Villarroya F, Villarroya J, Vincent O, Vindis C, Viret C, Viscomi MT, Visnjic D, Vitale I, Vocadlo DJ, Voitsekhovskaja OV, Volonté C, Volta M, Vomero M, Haefen CV, Vooijs MA, Voos W, Vucicevic L, Wade-Martins R, Waguri S, Waite KA, Wakatsuki S, Walker DW, Walker MJ, Walker SA, Walter J, Wandosell FG, Wang B, Wang C-Y, Wang C, Wang C, Wang C, Wang C-Y, Wang D, Wang F, Wang F, Wang F, Wang G, Wang H, Wang H, Wang H, Wang H-G, Wang J, Wang J, Wang J, Wang J, Wang K, Wang L, Wang L, Wang MH, Wang M, Wang N, Wang P, Wang P, Wang P, Wang P, Wang QJ, Wang Q, Wang QK, Wang QA, Wang W-T, Wang W, Wang X, Wang X, Wang Y, Wang Y, Wang Y, Wang Y-Y, Wang Y, Wang Y, Wang Y, Wang Y, Wang Z, Wang Z, Wang Z, Warnes G, Warnsmann V, Watada H, Watanabe E, Watchon M, Wawrzyńska A, Weaver TE, Wegrzyn G, Wehman AM, Wei H, Wei L, Wei T, Wei Y, Weiergräber OH, Weihl CC, Weindl G, Weiskirchen R, Wells A, Wen RH, Wen X, Werner A, Weykopf B, Wheatley SP, Whitton JL, Whitworth AJ, Wiktorska K, Wildenberg ME, Wileman T, Wilkinson S, Willbold D, Williams B, Williams RSB, Williams RL, Williamson PR, Wilson RA, Winner B, Winsor NJ, Witkin SS, Wodrich H, Woehlbier U, Wollert T, Wong E, Wong JH, Wong RW, Wong VKW, Wong WW-L, Wu A-G, Wu C, Wu J, Wu J, Wu KK, Wu M, Wu S-Y, Wu S, Wu S-Y, Wu S, Wu WKK, Wu X, Wu X, Wu Y-W, Wu Y, Xavier RJ, Xia H, Xia L, Xia Z, Xiang G, Xiang J, Xiang M, Xiang W, Xiao B, Xiao G, Xiao H, Xiao H-T, Xiao J, Xiao L, Xiao S, Xiao Y, Xie B, Xie C-M, Xie M, Xie Y, Xie Z, Xie Z, Xilouri M, Xu C, Xu E, Xu H, Xu J, Xu JR, Xu L, Xu WW, Xu X, Xue Y, Yakhine-Diop SMS, Yamaguchi M, Yamaguchi O, Yamamoto A, Yamashina S, Yan S, Yan S-J, Yan Z, Yanagi Y, Yang C, Yang D-S, Yang H, Yang H-T, Yang H, Yang J-M, Yang J, Yang J, Yang L, Yang L, Yang M, Yang P-M, Yang

Q, Yang S, Yang S, Yang S-F, Yang W, Yang WY, Yang X, Yang X, Yang Y, Yang Y, Yao H, Yao S, Yao X, Yao Y-G, Yao Y-M, Yasui T, Yazdankhah M, Yen PM, Yi C, Yin X-M, Yin Y, Yin Z, Yin Z, Ying M, Ying Z, Yip CK, Yiu SPT, Yoo YH, Yoshida K, Yoshii SR, Yoshimori T, Yousefi B, Yu B, Yu H, Yu J, Yu J, Yu L, Yu M-L, Yu S-W, Yu VC, Yu WH, Yu Z, Yu Z, Yuan J, Yuan L-Q, Yuan S, Yuan S-SF, Yuan Y, Yuan Z, Yue J, Yue Z, Yun J, Yung RL, Zacks DN, Zaffagnini G, Zambelli VO, Zanella I, Zang QS, Zanivan S, Zappavigna S, Zaragoza P, Zarbalis KS, Zarebkohan A, Zarrouk A, Zeitlin SO, Zeng J, Zeng J-D, Žerovnik E, Zhan L, Zhang B, Zhang DD, Zhang H, Zhang H, Zhang H, Zhang H, Zhang H, Zhang H, Zhang H-L, Zhang J, Zhang J, Zhang J-P, Zhang KYB, Zhang LW, Zhang L, Zhang L, Zhang L, Zhang M, Zhang P, Zhang S, Zhang W, Zhang X, Zhang X-W, Zhang X, Zhang X, Zhang X, Zhang X, Zhang XD, Zhang Y, Zhang Y, Zhang Y, Zhang Y-D, Zhang Y, Zhang Y-Y, Zhang Y, Zhang Z, Zhang Z, Zhang Z, Zhang Z, Zhang Z, Zhang Z, Zhao H, Zhao L, Zhao S, Zhao T, Zhao X-F, Zhao Y, Zhao Y, Zhao Y, Zhao Y, Zheng G, Zheng K, Zheng L, Zheng S, Zheng X-L, Zheng Y, Zheng Z-G, Zhivotovsky B, Zhong Q, Zhou A, Zhou B, Zhou C, Zhou G, Zhou H, Zhou H, Zhou H, Zhou J, Zhou J, Zhou J, Zhou J, Zhou K, Zhou R, Zhou X-J, Zhou Y, Zhou Y, Zhou Y, Zhou Z-Y, Zhou Z, Zhu B, Zhu C, Zhu G-Q, Zhu H, Zhu H, Zhu H, Zhu W-G, Zhu Y, Zhu Y, Zhuang H, Zhuang X, Zientara-Rytter K, Zimmermann CM, Ziviani E, Zoladek T, Zong W-X, Zorov DB, Zorzano A, Zou W, Zou Z, Zou Z, Zuryn S, Zwerschke W, Brand-Saberi B, Dong XC, Kenchappa CS, Li Z, Lin Y, Oshima S, Rong Y, Sluimer JC, Stallings CL, Tong C-K, Guidelines for the use and interpretation of assays for monitoring autophagy (4th edition)[1]. Autophagy 17, 1–382 (2021). [PubMed: 33634751]

18. Rai S, Manjithaya R, Fluorescence microscopy: A tool to study autophagy. AIP Adv. 5, 084804 (2015).
19. Turner APF, Biosensors: Fundamentals and applications - Historic book now open access. Biosens. Bioelectron. 65, A1 (2015). [PubMed: 25459061]
20. Marroqui L, Dos Santos RS, Op de Beeck A, Coomans de Brachene A, Marselli L, Marchetti P, Eizirik DL, Interferon-α mediates human beta cell HLA class I overexpression, endoplasmic reticulum stress and apoptosis, three hallmarks of early human type 1 diabetes. Diabetologia 60, 656–667 (2017). [PubMed: 28062922]
21. Coomans de Brachene A, Dos Santos RS, Marroqui L, Colli ML, Marselli L, Mirmira RG, Marchetti P, Eizirik DL, IFN-α induces a preferential long-lasting expression of MHC class I in human pancreatic beta cells. Diabetologia 61, 636–640 (2018). [PubMed: 29305625]
22. Kallionpaa H, Elo LL, Laajala E, Mykkanen J, Ricano-Ponce I, Vaarma M, Laajala TD, Hyoty H, Ilonen J, Veijola R, Simell T, Wijmenga C, Knip M, Lahdesmaki H, Simell O, Lahesmaa R, Innate immune activity is detected prior to seroconversion in children with HLA-conferred type 1 diabetes susceptibility. Diabetes 63, 2402–2414 (2014). [PubMed: 24550192]
23. Ferreira RC, Guo H, Coulson RM, Smyth DJ, Pekalski ML, Burren OS, Cutler AJ, Doecke JD, Flint S, McKinney EF, Lyons PA, Smith KG, Achenbach P, Beyerlein A, Dunger DB, Clayton DG, Wicker LS, Todd JA, Bonifacio E, Wallace C, Ziegler A-G, A type I interferon transcriptional signature precedes autoimmunity in children genetically at risk for type 1 diabetes. Diabetes 63, 2538–2550 (2014). [PubMed: 24561305]
24. Suzuki T, Matsuzaki T, Hagiwara H, Aoki T, Takata K, Recent advances in fluorescent labeling techniques for fluorescence microscopy. Acta Histochem. Cytochem. 40, 131–137 (2007). [PubMed: 18224244]
25. Rosado CJ, Mijaljica D, Hatzinisiriou I, Prescott M, Devenish RJ, Rosella: A fluorescent pH-biosensor for reporting vacuolar turnover of cytosol and organelles in yeast. Autophagy 4, 205–213 (2008). [PubMed: 18094608]
26. Iwashita H, Sakurai HT, Nagahora N, Ishiyama M, Shioji K, Sasamoto K, Okuma K, Shimizu S, Ueno Y, Small fluorescent molecules for monitoring autophagic flux. FEBS Lett. 592, 559–567 (2018). [PubMed: 29355929]
27. Man H, Zhou L, Zhu G, Zheng Y, Ye Z, Huang Z, Teng X, Ai C, Ge G, Xiao Y, Super-resolution imaging of autophagy by a preferred pair of self-labeling protein tags and fluorescent ligands. Anal. Chem. 94, 15057–15066 (2022). [PubMed: 36262049]
28. Mizushima N, Yoshimori T, Levine B, Methods in mammalian autophagy research. Cell 140, 313–326 (2010). [PubMed: 20144757]

29. Lichtman JW, Conchello JA, Fluorescence microscopy. Nat. Methods 2, 910–919 (2005). [PubMed: 16299476]
30. Kimura S, Noda T, Yoshimori T, Dissection of the autophagosome maturation process by a novel reporter protein, tandem fluorescent-tagged LC3. Autophagy 3, 452–460 (2007). [PubMed: 17534139]
31. N'Diaye EN, Kajihara KK, Hsieh I, Morisaki H, Debnath J, Brown EJ, PLIC proteins or ubiquilins regulate autophagy-dependent cell survival during nutrient starvation. EMBO Rep. 10, 173–179 (2009). [PubMed: 19148225]
32. Patterson GH, Knobel SM, Sharif WD, Kain SR, Piston DW, Use of the green fluorescent protein and its mutants in quantitative fluorescence microscopy. Biophys. J. 73, 2782–2790 (1997). [PubMed: 9370472]
33. Wu B, Chen Y, Muller JD, Fluorescence fluctuation spectroscopy of mCherry in living cells. Biophys. J. 96, 2391–2404 (2009). [PubMed: 19289064]
34. Cinelli RA, Ferrari A, Pellegrini V, Tyagi M, Giacca M, Beltram F, The enhanced green fluorescent protein as a tool for the analysis of protein dynamics and localization: Local fluorescence study at the single-molecule level. Photochem. Photobiol. 71, 771–776 (2000). [PubMed: 10857375]
35. Reissaus CA, Piñeros AR, Twigg AN, Orr KS, Conteh AM, Martinez MM, Kamocka MM, Day RN, Tersey SA, Mirmira RG, Dunn KW, Linnemann AK, Versatile A, Portable intravital microscopy platform for studying beta-cell biology in vivo. Sci. Rep. 9, 8449 (2019). [PubMed: 31186447]
36. Hohmeier HE, Mulder H, Chen G, Henkel-Rieger R, Prentki M, Newgard CB, Isolation of INS-1-derived cell lines with robust ATP-sensitive K+ channel-dependent and -independent glucose-stimulated insulin secretion. Diabetes 49, 424–430 (2000). [PubMed: 10868964]
37. Ravassard P, Hazhouz Y, Pechberty S, Bricout-Neveu E, Armanet M, Czernichow P, Scharfmann R, A genetically engineered human pancreatic β cell line exhibiting glucose-inducible insulin secretion. J. Clin. Invest. 121, 3589–3597 (2011). [PubMed: 21865645]
38. Lim H, Lim YM, Kim KH, Jeon YE, Park K, Kim J, Hwang HY, Lee DJ, Pagire H, Kwon HJ, Ahn JH, Lee MS, A novel autophagy enhancer as a therapeutic agent against metabolic syndrome and diabetes. Nat. Commun. 9, 1438 (2018). [PubMed: 29650965]
39. Park K, Lee MS, Current status of autophagy enhancers in metabolic disorders and other diseases. Front. Cell Dev. Biol. 10, 811701 (2022). [PubMed: 35237600]
40. Kabeya Y, Mizushima N, Ueno T, Yamamoto A, Kirisako T, Noda T, Kominami E, Ohsumi Y, Yoshimori T, LC3, a mammalian homologue of yeast Apg8p, is localized in autophagosome membranes after processing. EMBO J. 19, 5720–5728 (2000). [PubMed: 11060023]
41. Geeraert C, Ratier A, Pfisterer SG, Perdiz D, Cantaloube I, Rouault A, Pattingre S, Proikas-Cezanne T, Codogno P, Pous C, Starvation-induced hyperacetylation of tubulin is required for the stimulation of autophagy by nutrient deprivation. J. Biol. Chem. 285, 24184–24194 (2010). [PubMed: 20484055]
42. Goginashvili A, Zhang Z, Erbs E, Spiegelhalter C, Kessler P, Mihlan M, Pasquier A, Krupina K, Schieber N, Cinque L, Morvan J, Sumara I, Schwab Y, Settembre C, Ricci R, Insulin granules. Insulin secretory granules control autophagy in pancreatic β cells. Science 347, 878–882 (2015). [PubMed: 25700520]
43. Jung HS, Autophagy: Starved β-cells seem different from starved body. J. Diabetes Investig. 7, 169–170 (2016).
44. Yoshii SR, Mizushima N, Monitoring and measuring autophagy. Int. J. Mol. Sci. 18, 1865 (2017). [PubMed: 28846632]
45. Jiang P, Mizushima N, LC3- and p62-based biochemical methods for the analysis of autophagy progression in mammalian cells. Methods 75, 13–18 (2015). [PubMed: 25484342]
46. Slater AF, Chloroquine: Mechanism of drug action and resistance in *Plasmodium falciparum*. Pharmacol. Ther. 57, 203–235 (1993). [PubMed: 8361993]
47. Homewood CA, Warhurst DC, Peters W, Baggaley VC, Lysosomes, pH and the anti-malarial action of chloroquine. Nature 235, 50–52 (1972). [PubMed: 4550396]
48. Schmeisser H, Bekisz J, Zoon KC, New function of type I IFN: Induction of autophagy. J. Interferon Cytokine Res. 34, 71–78 (2014). [PubMed: 24428799]

49. Tian Y, Wang M-L, Zhao J, Crosstalk between autophagy and Type I interferon responses in innate antiviral immunity. Viruses 11, 132 (2019). [PubMed: 30717138]
50. Martin KR, Barua D, Kauffman AL, Westrate LM, Posner RG, Hlavacek WS, Mackeigan JP, Computational model for autophagic vesicle dynamics in single cells. Autophagy 9, 74–92 (2013). [PubMed: 23196898]
51. Han K, Kim SH, Choi M, Computational modeling of the effects of autophagy on amyloid-β peptide levels. Theor. Biol. Med. Model. 17, 2 (2020). [PubMed: 32102666]
52. Mai S, Muster B, Bereiter-Hahn J, Jendrach M, Autophagy proteins LC3B, ATG5 and ATG12 participate in quality control after mitochondrial damage and influence lifespan. Autophagy 8, 47–62 (2012). [PubMed: 22170153]
53. Walczak M, Martens S, Dissecting the role of the Atg12-Atg5-Atg16 complex during autophagosome formation. Autophagy 9, 424–425 (2013). [PubMed: 23321721]
54. Black S, Phillips D, Hickey JW, Kennedy-Darling J, Venkataraaman VG, Samusik N, Goltsev Y, Schurch CM, Nolan GP, CODEX multiplexed tissue imaging with DNA-conjugated antibodies. Nat. Protoc. 16, 3802–3835 (2021). [PubMed: 34215862]
55. Chen D, Thayer TC, Wen L, Wong FS, Mouse models of autoimmune diabetes: The nonobese diabetic (NOD) mouse. Methods Mol. Biol. 2128, 87–92 (2020). [PubMed: 32180187]
56. Chen YG, Mathews CE, Driver JP, The role of NOD mice in type 1 diabetes research: Lessons from the past and recommendations for the future. Front. Endocrinol. 9, 51 (2018).
57. Wagner LE, Melnyk O, Duffett BE, Linnemann AK, Mouse models and human islet transplantation sites for intravital imaging. Front. Endocrinol. 13, 992540 (2022).
58. Arrojo EDR, Roy B, MacDonald PE, Molecular and functional profiling of human islets: From heterogeneity to human phenotypes. Diabetologia 63, 2095–2101 (2020). [PubMed: 32894320]
59. Oram RA, Sims EK, Evans-Molina C, Beta cells in type 1 diabetes: Mass and function; sleeping or dead? Diabetologia 62, 567–577 (2019). [PubMed: 30767048]
60. Mallone R, Eizirik DL, Presumption of innocence for beta cells: Why are they vulnerable autoimmune targets in type 1 diabetes? Diabetologia 63, 1999–2006 (2020). [PubMed: 32894310]
61. Toren E, Burnette KS, Banerjee RR, Hunter CS, Tse HM, Partners in crime: Beta-cells and autoimmune responses complicit in type 1 diabetes pathogenesis. Front. Immunol. 12, 756548 (2021). [PubMed: 34691077]
62. Moon S, Jung HS, Endoplasmic reticulum stress and dysregulated autophagy in human pancreatic Beta cells. Diabetes Metab. J. 46, 533–542 (2022). [PubMed: 35929171]
63. Muralidharan C, Linnemann AK, β-Cell autophagy in the pathogenesis of type 1 diabetes. Am. J. Physiol. Endocrinol. Metab. 321, E410–E416 (2021). [PubMed: 34338043]
64. Moulis M, Vindis C, Methods for measuring autophagy in mice. Cells 6, 14 (2017). [PubMed: 28594368]
65. Adams MT, Dwulet JM, Briggs JK, Reissaus CA, Jin E, Szulczewski JM, Lyman MR, Sdao SM, Kravets V, Nimkulrat SD, Ponik SM, Merrins MJ, Mirmira RG, Linnemann AK, Benninger RK, Blum B, Reduced synchroneity of intra-islet Ca^{2+} oscillations in vivo in Robo-deficient β cells. eLife 10, e61308 (2021). [PubMed: 34231467]
66. Georgiadou E, Muralidharan C, Martinez M, Chabosseau P, Akalestou E, Tomas A, Wern FYS, Stylianides T, Wretlind A, Legido-Quigley C, Jones B, Lopez-Noriega L, Xu Y, Gu G, Alsabeeh N, Cruciani-Guglielmacci C, Magnan C, Ibberson M, Leclerc I, Ali Y, Soleimanpour SA, Linnemann AK, Rodriguez TA, Rutter GA, Mitofusins Mfn1 and Mfn2 are required to preserve glucose- but not incretin-stimulated beta-cell connectivity and insulin secretion. Diabetes 71, 1472–1489 (2022). [PubMed: 35472764]
67. Marasco MR, Conteh AM, Reissaus CA, Cupit V JE, Appleman EM, Mirmira RG, Linnemann AK, Interleukin-6 reduces β-cell oxidative stress by linking autophagy with the antioxidant response. Diabetes 67, 1576–1588 (2018). [PubMed: 29784660]
68. Lambelet M, Terra LF, Fukaya M, Meyerovich K, Labriola L, Cardozo AK, Allagnat F, Dysfunctional autophagy following exposure to pro-inflammatory cytokines contributes to pancreatic β-cell apoptosis. Cell Death Dis. 9, 96 (2018). [PubMed: 29367588]
69. Mizushima N, Kuma A, Autophagosomes in GFP-LC3 transgenic mice. Methods Mol. Biol. 445, 119–124 (2008). [PubMed: 18425446]

70. Aoyama S, Nishida Y, Uzawa H, Himuro M, Kanai A, Ueki K, Ito M, Iida H, Tanida I, Miyatsuka T, Fujitani Y, Matsumoto M, Watada H, Monitoring autophagic flux in vivo revealed its physiological response and significance of heterogeneity in pancreatic beta cells. Cell Chem. Biol. 30, 658–671.e4 (2023). [PubMed: 36944338]
71. Kamitani M, Miyatsuka T, Miura M, Azuma K, Suzuki L, Himuro M, Katahira T, Nishida Y, Fujitani Y, Watada H, Heterogeneity of autophagic status in pancreatic β cells under metabolic stress. Biochem. Biophys. Res. Commun. 496, 328–334 (2018). [PubMed: 29337057]
72. Ritsma L, Steller EJ, Ellenbroek SI, Kranenburg O, Borel Rinkes IH, van Rheenen J, Surgical implantation of an abdominal imaging window for intravital microscopy. Nat. Protoc. 8, 583–594 (2013). [PubMed: 23429719]
73. Park I, Hong S, Hwang Y, Kim P, A novel pancreatic imaging window for stabilized longitudinal in vivo observation of pancreatic islets in murine model. Diabetes Metab. J. 44, 193–198 (2020). [PubMed: 31237131]
74. Wang Z, Zhu T, Rehman KK, Bertera S, Zhang J, Chen C, Papworth G, Watkins S, Trucco M, Robbins PD, Li J, Xiao X, Widespread and stable pancreatic gene transfer by adeno-associated virus vectors via different routes. Diabetes 55, 875–884 (2006). [PubMed: 16567506]
75. Ravier MA, Daro D, Roma LP, Jonas JC, Cheng-Xue R, Schuit FC, Gilon P, Mechanisms of control of the free Ca^{2+} concentration in the endoplasmic reticulum of mouse pancreatic β-cells: Interplay with cell metabolism and $[Ca^{2+}]_c$ and role of SERCA2b and SERCA3. Diabetes 60, 2533–2545 (2011). [PubMed: 21885870]
76. Stull ND, Breite A, McCarthy R, Tersey SA, Mirmira RG, Mouse islet of Langerhans isolation using a combination of purified collagenase and neutral protease. J. Vis. Exp. 2012, 4137 (2012).
77. Hogrebe NJ, Maxwell KG, Augsornworawat P, Millman JR, Generation of insulin-producing pancreatic beta cells from multiple human stem cell lines. Nat. Protoc. 16, 4109–4143 (2021). [PubMed: 34349281]
78. Benninger RK, Hao M, Piston DW, Multi-photon excitation imaging of dynamic processes in living cells and tissues. Rev. Physiol. Biochem. Pharmacol. 160, 71–92 (2008). [PubMed: 18418560]
79. Franke T, Rhode S, Two-photon microscopy for deep tissue imaging of living specimens. Micros. Today 20, 12–16 (2012).
80. Schindelin J, Arganda-Carreras I, Frise E, Kaynig V, Longair M, Pietzsch T, Preibisch S, Rueden C, Saalfeld S, Schmid B, Tinevez JY, White DJ, Hartenstein V, Eliceiri K, Tomancak P, Cardona A, Fiji: An open-source platform for biological-image analysis. Nat. Methods 9, 676–682 (2012). [PubMed: 22743772]
81. Goltsev Y, Samusik N, Kennedy-Darling J, Bhate S, Hale M, Vazquez G, Black S, Nolan GP, Deep profiling of mouse splenic architecture with CODEX multiplexed imaging. Cell 174, 968–981.e15 (2018). [PubMed: 30078711]
82. Cabrera SM, Colvin SC, Tersey SA, Maier B, Nadler JL, Mirmira RG, Effects of combination therapy with dipeptidyl peptidase-IV and histone deacetylase inhibitors in the non-obese diabetic mouse model of type 1 diabetes. Clin. Exp. Immunol. 172, 375–382 (2013). [PubMed: 23600825]
83. Apaolaza PS, Petropoulou PI, Rodriguez-Calvo T, Whole-slide image analysis of human pancreas samples to elucidate the immunopathogenesis of type 1 diabetes using the QuPath software. Front. Mol. Biosci. 8, 689799 (2021). [PubMed: 34179094]

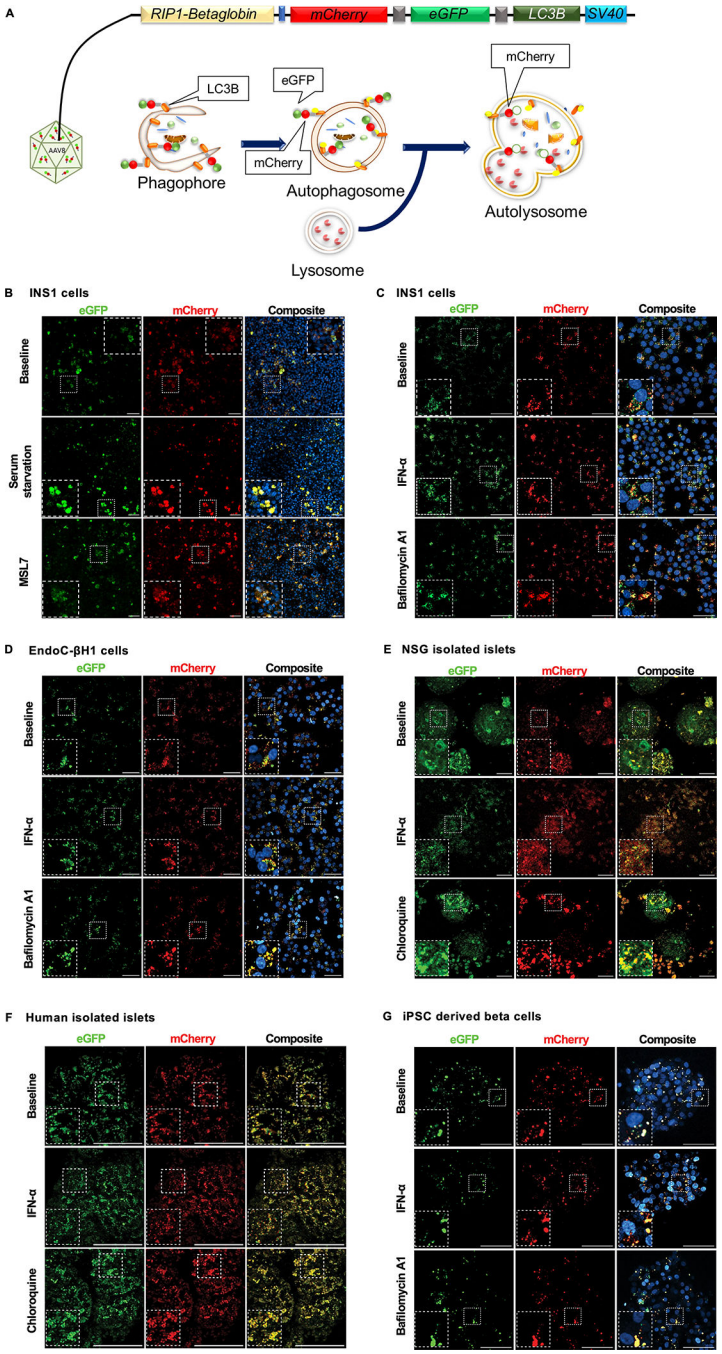

Fig. 1. Autophagy biosensor successfully labels the autophagosomal membrane and functions as expected in β cells in vitro.

(**A**) Schematic showing the macroautophagy process with AAV8-LC3B-eGFP-mCherry biosensor–binding site and expected fluorescence change. (**B**) Qualitative images of INS-1 cells transduced with the autophagy sensor at an MOI of 5000 and then serum-starved in HBSS or treated with the autophagy-stimulating compound MSL7 over a 3-hour time course. (**C**) Qualitative images of INS-1 cells transduced with 5000 MOI of the autophagy biosensor and then treated with the autophagy inhibitor bafilomycin A1 and

proinflammatory cytokine IFN-α. (**D**) Qualitative images of endo-CβH1 cells transduced with 5000 MOI of the autophagy biosensor and then treated with the autophagy inhibitor bafilomycin A1 and proinflammatory cytokine IFN-α. (**E**) Qualitative images of isolated islets from NSG mice transduced with 5000 MOI of the autophagy biosensor and then treated with the autophagy inhibitor CQ and proinflammatory cytokine IFN-α. (**F**) Qualitative images of isolated human islets transduced with 5000 MOI of the autophagy biosensor and then treated with the autophagy inhibitor CQ and proinflammatory cytokine IFN-α. (**G**) Qualitative images of iPSC-derived β cells transduced with 5000 MOI of the autophagy biosensor and then treated with the autophagy inhibitor bafilomycin A1 and proinflammatory cytokine IFN-α. The enlarged site is shown in the frame for each image. Scale bars, 50 μm.

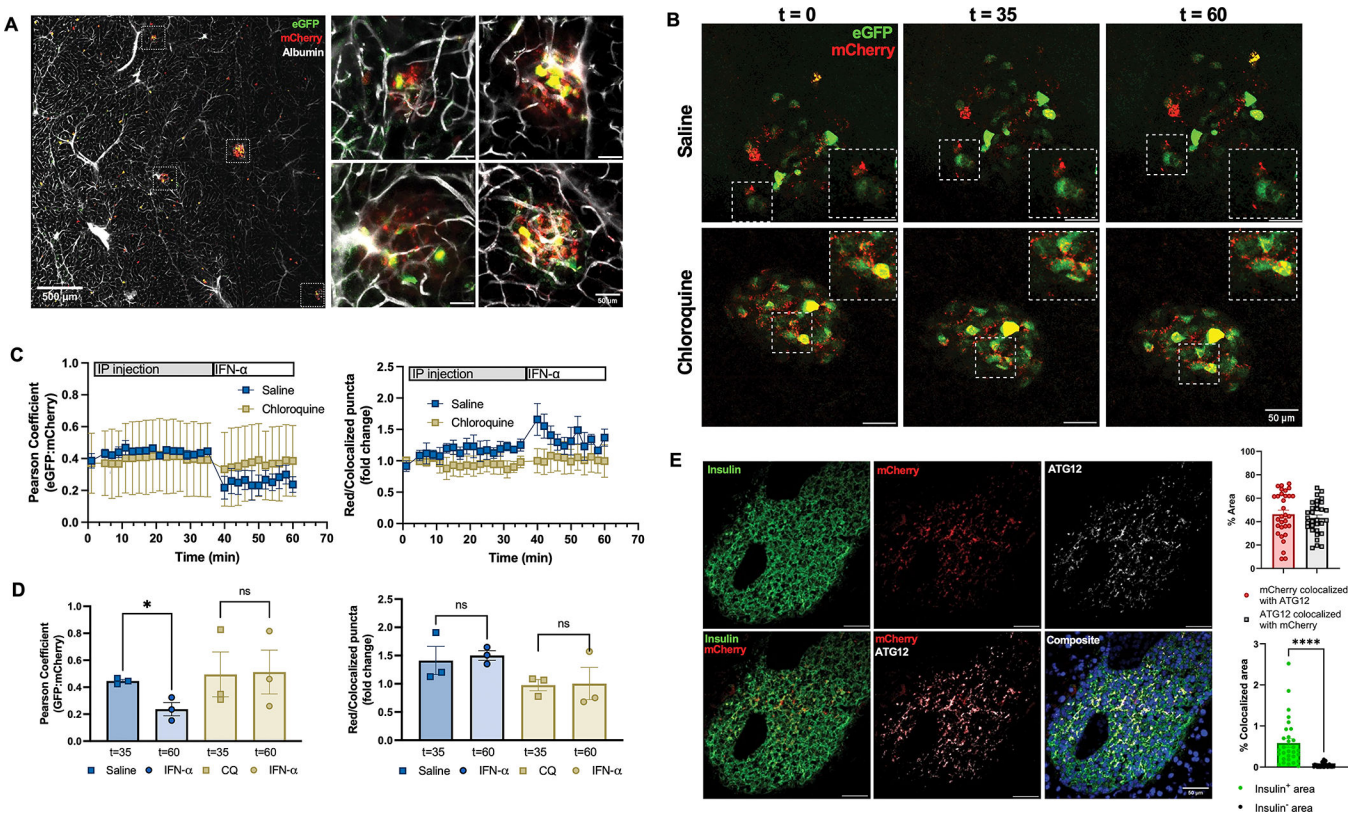

Fig. 2. The autophagy biosensor effectively measures autophagic flux in wild-type mice.

(**A**) Tiled representative image of a large area of a C57BL/6J mouse pancreas expressing the AAV8-packaged autophagy biosensor, with multiple islets identified. Individual islets (white dashed line boxes) are enlarged as maximum intensity projections of the collected z-stacks. Scale bars, 500 µm (left) and 50 µm (right). (**B**) Representative images of islets at various time points during intravital imaging. $t = 35$ is representative of basal exposure to either saline or CQ as indicated, whereas $t = 60$ is representative of the same islet after IFN-α is added after the saline or CQ exposure. Selected cells (white dashed line boxes) are enlarged in the corner of each image. Scale bars, 50 µm. (**C**) Quantitative analysis of autophagic flux in wild-type mice. Pearson correlation coefficient and the punctum count in the form of red/colocalized punctum ratio fold change are shown for mice injected with either saline followed by IFN-α or CQ followed by IFN-α. (**D**) Statistical comparison of the Pearson correlation coefficient and the punctum count at the end time points of saline/CQ and IFN-α treatment. (**E**) Representative images of islets in pancreas sections from C57BL/6J mice after intravital imaging stained for insulin and ATG12, with quantification of the colocalized area of mCherry and ATG12 on the insulin-positive/negative area of the islet. Scale bars, 50 µm. Data points are mean ± SEM, $n = 3$ animals per condition. Data were analyzed by Student's t test; $^{*}P < 0.05$ and $^{****}P < 0.001$; ns, not significant. ip, intraperitoneal.

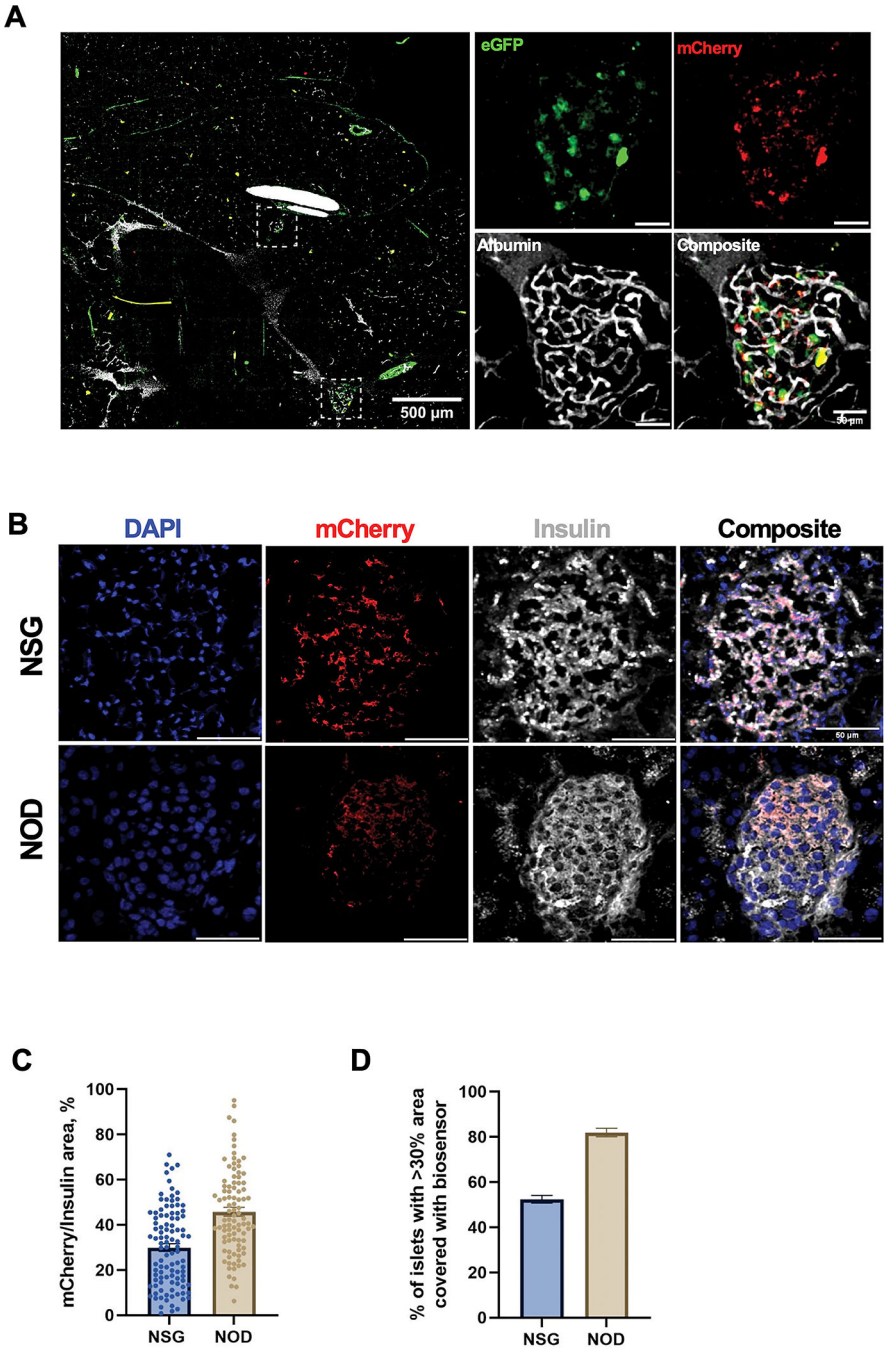

Fig. 3. NOD and NSG β cells efficiently express the autophagy biosensor.

(**A**) Intravital image of a large area of biosensor-infected NSG mouse pancreas with two individual islets denoted (white dashed line boxes). One islet is shown at higher resolution as a maximum projection of the collected z-stack. Scale bars, 500 μm (left) and 50 μm (right). (**B**) Representative images of islets in pancreas sections from female NSG and NOD mice after intravital imaging. Scale bars, 50 μm. (**C**) Quantification of (B) showing the proportion of β cells in a given islet that are also expressing biosensor (i.e., the mCherry-positive area). Each point represents a single islet. Means ± SEM are shown for $n = 6$ mice per group. (**D**)

Quantification of the per-centages of the islets throughout the pancreas expressing biosensor in at least 30% of the β cells. Means ± SEM are shown for $n = 6$ mice per group.

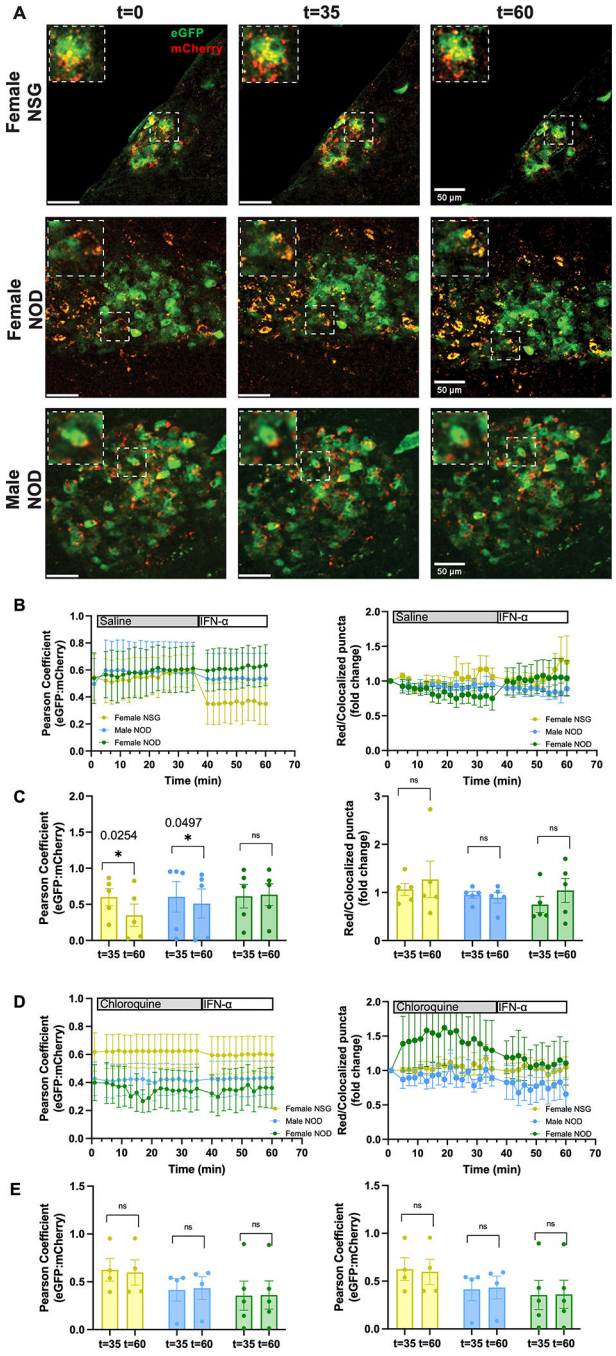

Fig. 4. Autophagic flux is impaired in female NOD mice.

(**A**) Representative images of the analyzed islets are shown for female NSG, female NOD, and male NOD mice after saline (t = 35 min) and IFN-α (t = 60 min) injections. Single-cell images depicted in the frames are enlarged. Scale bars, 50 μm. (**B**) Quantitative analysis of autophagic flux is shown for female NSG, female NOD, and male NOD mice after saline and IFN-α injections. (**C**) Statistical comparison of the Pearson correlation coefficient and the punctum count at the end time points of saline and IFN-α treatments. Pearson correlation coefficient as a function of time and red/colocalized punctum fold change over

time is shown. Means ± SEM are plotted for each animal strain. $n = 4$ or 5 for each strain, one or two islets per animal analyzed. (**D**) Quantitative analysis of autophagic flux after CQ and IFN-α injection is shown. (**E**) Statistical comparison of the Pearson correlation coefficient and the punctum count at the end time points of CQ and IFN-α treatment. Pearson correlation coefficient as a function of time and red/colocalized punctum fold change over time is shown. Means ± SEM are plotted in (B) to (E) with Student's *t* test performed for statistical analyses in (C) and (E); $n = 4$ or 5 animals per strain with one or two islets per animal analyzed. $^*P < 0.05$.

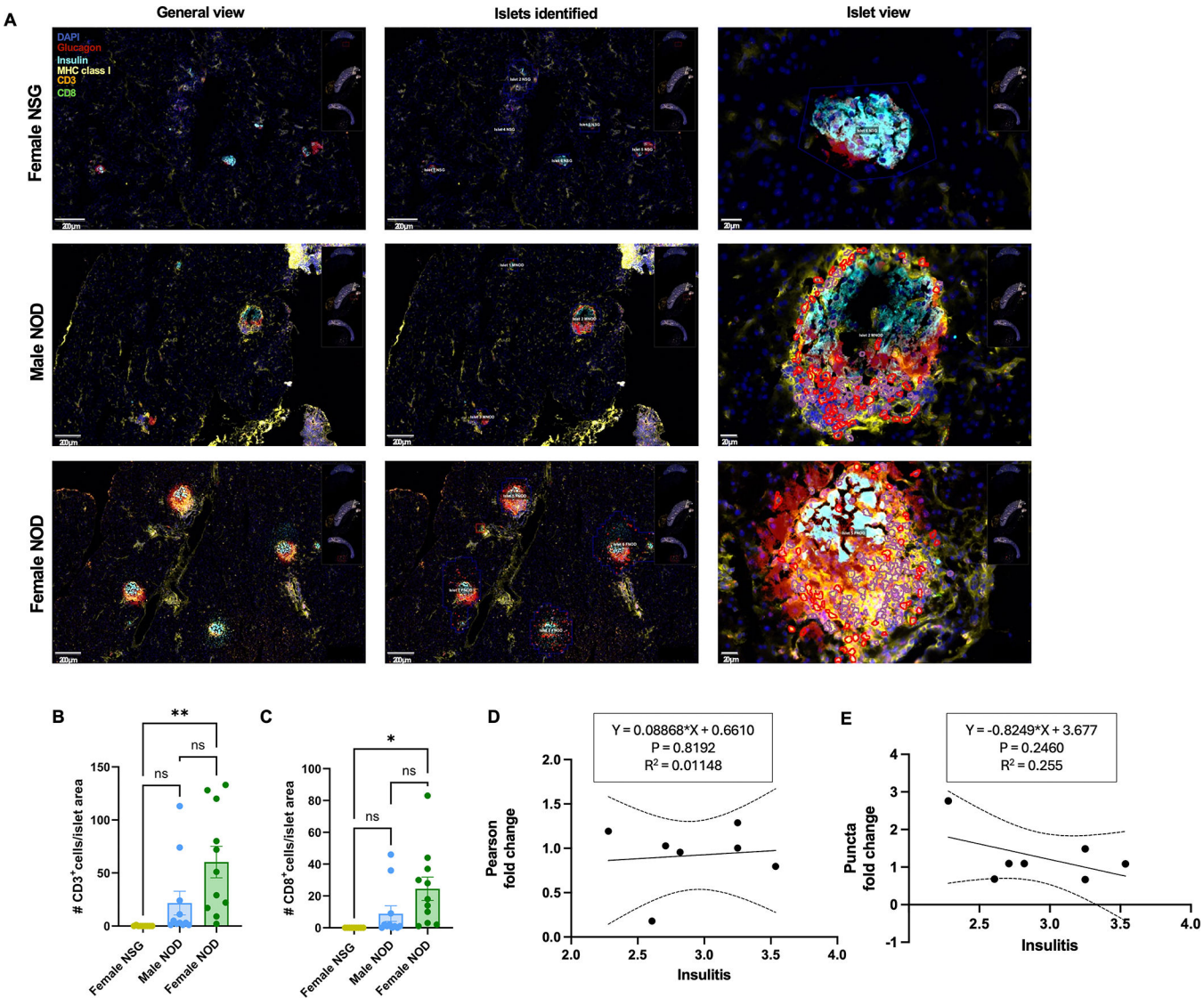

Fig. 5. Insulitis in male and female NOD mice broadly correlates with in vivo autophagic flux.

(**A**) Set of overview images collected after CODEX panel to evaluate the pancreata of female NSG, female NOD, and male NOD mice after intravital imaging. Inserts on the right show whole scanning area overview. Single-islet views show different cells identified for quantification. $CD3^+$ cells are shown with red margins, and $CD8^+$ cells are shown in purple. Scale bars, 200 μm (left and middle) and 20 μm (right). (**B**) The quantitative analysis of $CD3^+$ cells per islet is shown and compared between strains with the one-way ANOVA test, where each dot represents immune cells in a single islet. (**C**) The quantitative analysis of $CD8^+$ cells per islet is shown and compared between strains with the one-way ANOVA test, again where each dot represents immune cells in a single islet. Data in (B) and (C) are presented as mean ± SEM and were analyzed by one-way ANOVA with Tukey multiple comparisons test; $*P < 0.05$ and $**P < 0.01$. $n = 9$ to 11 islets from one representative animal in each group. (**D**) Spearman correlation between insulitis score and the Pearson coefficient fold change (IFN-α/saline) obtained from intravital imaging for the

male and female NOD mice. Each point represents data from a single animal. (**E**) Spearman correlation between insulitis score and the red/colocalized punctum metric (IFN-α/saline) obtained from intravital imaging for the same mice as in (D) where, again, each point represents data from a single animal. The solid lines in (D) and (E) indicate the fitted linear regression, with 95% confidence bands shown as dashed lines.

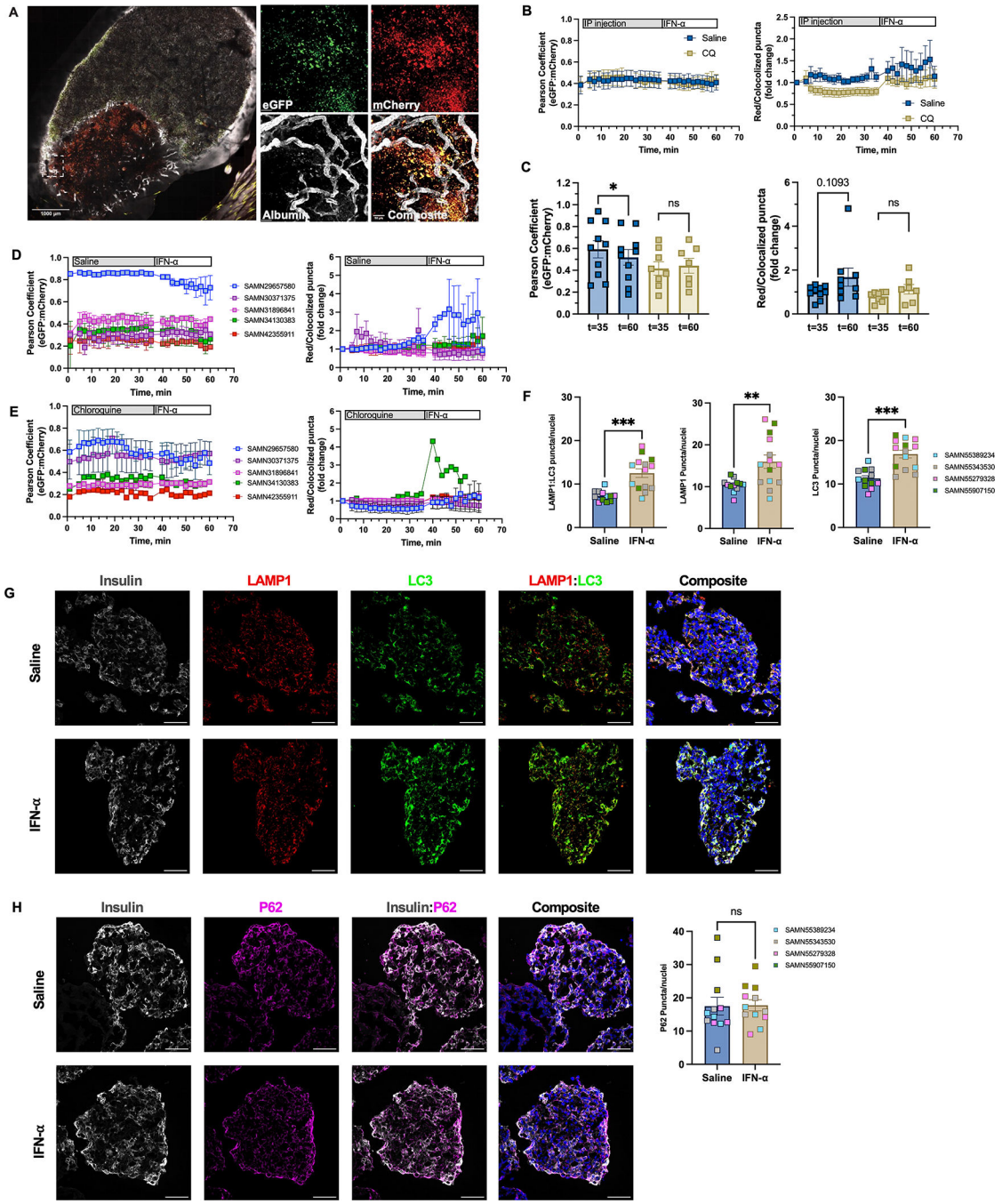

Fig. 6. Human islet autophagic flux is heterogeneous in vivo.

(**A**) Representative large-scale image of an NSG mouse kidney containing transplanted human islets infected with the autophagy biosensor with a region of interest (white dashed line box) further highlighted to show the EGFP (green) and mCherry (red) of the biosensor. The vascular network in and around the islets is labeled by albumin conjugated to Alexa Fluor 647 (white). Scale bars, 1000 μm (left) and 50 μm (right). (**B**) Quantitative analysis of autophagosomes (left) and autolysosomes (right) in all donor islets exposed to saline followed by IFN-α (blue) or CQ followed by IFN-α (gold). (**C**) Statistical comparison

of the Pearson correlation coefficient and the punctum count at the end time points of saline/CQ and IFN-α treatments. Means ± SEM are shown for $n = 5$ donors, with data representative of two mice per donor per condition. (**D**) Quantitative analysis of autophagosomes (left) and autolysosomes (right) separated by individual donor showing response to saline followed by IFN-α. Means ± SEM are shown for each donor. (**E**) Quantitative analysis of autophagosomes (left) and autolysosomes (right) separated by individual donor showing response to CQ followed by IFN-α. Means ± SEM are shown for each donor. (**F**) Quantification of LAMP1:LC3 colocalization (left), LAMP1 puncta (middle), and LC3 puncta (right) in the insulin-positive area of human islets after saline or IFN-α treatment. Each point is representative of a single islet. Means ± SEM are shown for $n = 4$ donors, with $n = 2$ to 4 islets per donor, per condition. (**G**) Representative immunofluorescence images of human islets stained for insulin (white), LAMP1 (red), and LC3 (green) under saline and IFN-α conditions, with merged images. Nuclei are stained with DAPI (blue). Scale bars, 50 μm. (**H**) Representative immunofluorescence images of human islets stained for insulin (white) and p62 (magenta). Nuclei are stained with DAPI (blue). Scale bars, 50 μm. Quantification of p62 signal in the insulin-positive area (right). Each point is representative of a single islet. Means ± SEM are shown for $n = 4$ donors, with $n = 2$ to 4 islets per donor, per condition. Student's t test was performed in (C), (F), and (H); $^{*}P < 0.05$, $^{**}P < 0.005$, and $^{***}P < 0.001$.

Table 1. Human organ donor information.

Phenotypic information for each donor, including sex, age, body mass index (BMI), and glycated hemoglobin (HbA1c), is provided. M, male; F, female.

Donor ID	Diabetes	Age	Sex	BMI	HbA1c
SAMN29657580	None	40	M	23	5.2
SAMN30371375	None	66	M	29.6	5.4
SAMN31896841	None	66	F	27.4	5.4
SAMN33456515	None	48	M	24.9	5.8
SAMN34076484	None	54	F	27.5	5.8
SAMN34075901	None	39	M	41.8	5.5
SAMN34130383	None	42	F	29.2	5.2
SAMN42355911	None	64	M	29.5	5.7
SAMN55279328	None	22	F	31.6	5.1
SAMN55343530	None	53	F	34.3	4.5
SAMN55389234	None	66	M	24.6	4.1
SAMN55907150	None	57	M	27.9	5.5